NACA

RESEARCH MEMORANDUM

BUFFET TESTS OF AN ATTACK-AIRPLANE MODEL WITH EMPHASIS

ON ANALYSIS OF DATA FROM WIND-TUNNEL TESTS

By Don D. Davis, Jr., and Dewey E. Wornom

Langley Aeronautical Laboratory
Langley Field, Va.

Declassified September 27, 1962

NATIONAL ADVISORY COMMITTEE
FOR AERONAUTICS
WASHINGTON

February 21, 1958

NATIONAL ADVISORY COMMITTEE FOR AERONAUTICS

RESEARCH MEMORANDUM

BUFFET TESTS OF AN ATTACK-AIRPLANE MODEL WITH EMPHASIS

ON ANALYSIS OF DATA FROM WIND-TUNNEL TESTS

By Don D. Davis, Jr., and Dewey E. Wornom

SUMMARY

The buffet characteristics of a 1/10-scale model of an attack airplane have been investigated at Mach numbers from 0.80 to 1.00. The wing had a modified delta plan form with an NACA 0008 (modified) airfoil section at the root and an NACA 0005 (modified) airfoil section at the tip, a leading-edge sweep of 41.11°, an aspect ratio of 2.91, and a taper ratio of 0.226. Modifications to the basic configuration included a tapered wing-leading-edge extension with camber, an addition to the wing trailing edge sweeping it forward 10°, and an area addition to the rearward fuselage section. In the speed range where the buffet boundary of the basic configuration was lowest, the buffet intensity was reduced substantially when these modifications were added to the model.

During buffet, the wing vibrated primarily in the first symmetrical mode. The damping of the vibration was not primarily aerodynamic as is the case for airplanes in flight at these speeds but, instead, was mostly structural apparently because of friction in a dovetail joint. As a result, any attempt to predict flight buffet stresses from the results of this investigation must be based on an estimate of the aerodynamic damping for the airplane.

A technique is described for making wind-tunnel buffet measurements and for deducing the system damping from the power spectrum of the wing vibration. Equations are derived for the buffet response of a platelike wing, the structural characteristics of which are described by mass and flexibility-influence-coefficient matrices.

For the mathematical model of the buffeting wing there is a relationship that connects the band width, the peak response, and the mean-square response. The experimental results show that this same relationship holds for the actual buffeting wing.

In designing buffet models, it is desirable to keep the structural damping very low, because the aerodynamic damping ratio is much lower for solid metal model wings than for actual airplane wings.

INTRODUCTION

Several attempts have been made to establish a correlation between the buffet boundary of an airplane and some quantity that is observable in wind-tunnel tests of a model. Certain quantities associated with the static lift characteristics have been used with some success for this purpose (refs. 1 and 2), as have measurements of wake-pressure fluctuations (ref. 3). The buffeting of models has also been observed directly by placing strain gages on the wings (ref. 3). With the aid of strain gages and modern data-handling techniques, it has recently become possible to give serious consideration to the more difficult problem of predicting, from wind-tunnel data, the loads that will be encountered during buffeting in flight.

The suggestion is made in reference 4 that the methods of generalized harmonic analysis can be applied to the problem of airplane buffet. Analyses of flight buffet data have since indicated the validity of this approach (refs. 5 and 6). By using these same techniques, a method has been derived for predicting flight buffet loads from model tests in a wind tunnel. Two comparisons between flight and wind-tunnel data are presented in reference 7 and the correlation, while perhaps not entirely adequate, is certainly very encouraging.

The primary purpose of the present buffet investigation was to make a wind-tunnel study of the buffet characteristics of a model of an attack airplane and, in particular, to evaluate the effects of certain modifications on the buffet characteristics. The tests were conducted at Mach numbers from 0.80 to 1.00 in the Langley 8-foot transonic pressure tunnel.

The instrumentation that was used was in accordance with the method of reference 7, and the tests were designed in such a way as to provide a check on some of the assumptions of that reference. The results show that an important assumption regarding the system damping did not apply in this test. Consequently, a large part of this paper is devoted to determining why this assumption did not apply, and to presenting the analysis techniques that were developed to circumvent this difficulty. This material is of particular interest to those readers who will be required to conduct buffet tests or to interpret the results of such tests.

SYMBOLS

$|A(\omega)|^2$ square of absolute value of system admittance

$[A]$ matrix of flexibility influence coefficients

b   wing span, ft

c   wing chord, ft

c_{av} average chord, $\frac{S}{b}$, ft

C_L lift coefficient, $\frac{\text{Lift}}{qS}$

$C_{L\alpha,1}$ first-mode generalized lift-curve slope for damping com-
                     ponent of aerodynamic force due to wing vibration,

$$\frac{\sum_{m} k_m s_m \left(\varphi_m(1)\right)^2}{S_2}, \text{ per radian}$$

$C_{N,1}$ generalized normal-force coefficient for first-mode
                     vibration, $\frac{N_1}{qS_1}$

f   frequency, cps

f_1 natural frequency of first symmetrical wing mode, cps

F_o amplitude of force exciting vibration, lb

F_S dimensionless structural factor, $\dfrac{M_{m,1}}{M_1 \frac{b}{2}} \sqrt{\dfrac{\pi S_1{}^2 M_1}{8 S_2 S M_W}}$

g   structural damping factor

k_m constant relating the damping component of local pressure
                     differential due to wing vibration to local angle of
                     attack (in radians) and free-stream dynamic pressure

k_S physical factor, $\omega_1 \frac{b}{2} \sqrt{c_{av} S M_W}$, ft^2-lb$^{1/2}$

L_1 generalized damping constant for first-mode wing vibra-
                     tion, $\frac{\text{lb-sec}}{\text{ft}}$

m   mass, slugs

$m(y)$ wing mass per unit span, slugs/ft

m_m mass of an element of the wing, slugs

M free-stream Mach number

$[M]$ diagonal inertia matrix for wing, made up of the elements m_m

$M_{m,1}$ effective moment (for first-mode vibration) of mass outboard of point y_g, $\displaystyle\int_{y_g}^{b/2} (y - y_g)m(y)w_1(y)dy$, slug-ft

M_n generalized wing mass for nth-mode vibration,
$$\sum_m m_m\left(\varphi_m{}^{(n)}\right)^2 \quad \text{or} \quad \int_{-b/2}^{b/2} m(y)w_n{}^2(y)dy, \text{ slugs}$$

M_W mass of wing, $\displaystyle\sum_m m_m \quad \text{or} \quad 2\int_0^{b/2} m(y)dy$, slugs

n integer denoting wing vibration mode

N_1 time-dependent generalized (for first-mode vibration) buffet force acting on wing, $\displaystyle\sum_m \Delta p_m s_m \varphi_m{}^{(1)}$, lb

$\{P\}$ column matrix representing a set of static loads applied to wing

Δp_m local pressure difference (between bottom and top surfaces of wing) that excites the buffet vibration

q free-stream dynamic pressure, lb/sq ft

R Reynolds number based on mean aerodynamic chord of 12.96 in.

r_n time-dependent displacement of wing element for which $\varphi^{(n)} = 1$

S wing area, sq ft

S_1 weighted wing area for first-mode bending,
$$\sum_m s_m \varphi_m{}^{(1)} \quad \text{or} \quad 2\int_0^{b/2} c(y)w_1(y)dy, \text{ sq ft}$$

S_2 weighted wing area for first-mode bending,
$$\sum_m s_m\left(\varphi_m{}^{(1)}\right)^2 \quad \text{or} \quad 2\int_0^{b/2} c(y)w_1{}^2(y)dy, \text{ sq ft}$$

s_m area of mth element of wing, sq ft

t time, sec

T kinetic energy of vibrating system, lb-ft

$[U]$ dynamic matrix for wing, $[A]\ [M]$

V free-stream velocity, ft/sec

$w_n(y)$ deflection of wing elastic axis in nth wing bending
                 mode, normalized to unit deflection at the wing tip

y spanwise distance from fuselage center line, ft

y_g spanwise distance from fuselage center line to strain-gage
                 location, ft

z vertical displacement

z_m time-dependent displacement of the mth wing element, ft

α angle of attack, deg or radians

β phase angle by which displacement lags the force

γ aerodynamic damping ratio based on critical damping,
$$\frac{C_{L_\alpha,1}qS_2}{2M_1\omega_1V}$$

ρ air density

σ root-mean-square value

$\varphi_m{}^{(n)}$ normalized deflection of mth wing element for wing vibra-
                 tion in the nth normal mode

Φ power spectral density

ω circular frequency, $2\pi f$, radians/sec

ω_n undamped natural circular frequency for nth mode

ω_r resonant frequency

Ω frequency ratio, ω/ω_n

Ω_r resonant frequency ratio, ω_r/ω_n

$\Omega_{1/2}$ frequency ratio at half-power point

$\Delta\Omega$ difference between frequency ratio at half-power point
                  above Ω_r and frequency ratio at half-power point
                  below Ω_r

Subscripts:

M   buffet bending moment

n   nth natural mode, where n is any integer

r   at resonance

   Dots over symbols denote derivatives with respect to time.

APPARATUS AND TESTS

Tunnel

   The investigation was conducted in the Langley 8-foot transonic pressure tunnel which is a single-return tunnel with a rectangular slotted test section (fig. 1) capable of permitting continuous operation through the transonic speed range at stagnation pressures from 1/4 to 1 atmosphere. Automatic temperature controls maintained a constant and uniform stagnation temperature of 120° F during the tests. In order to prevent condensation, the dew point was maintained at 0° F or lower.

   Local Mach number distributions over the test-section length occupied by the model are shown in figure 2. These distributions were obtained at a stagnation pressure of 1 atmosphere from a multiorifice axial survey tube on the tunnel center line. Changes in stagnation pressure have essentially

no effect on the Mach number distributions. The design of the sting-support system, figure 1, is such that the model remains near the center line of the test section throughout the angle-of-attack range.

Model

Tests were performed with a 1/10-scale model of an attack airplane. A three-view drawing of the model is shown in figure 3. The modified delta wing, made of 24ST aluminum alloy, had an NACA 0008 (modified) airfoil section at the root and an NACA 0005 (modified) airfoil section at the tip, a leading-edge sweep of 41.11°, an aspect ratio of 2.91, and a taper ratio of 0.226.

Modifications to the basic configuration included a tapered wing-leading-edge extension with camber, an addition to the wing trailing edge sweeping it forward 10°, and an area addition to the rearward fuselage section. A drawing of the basic wing and the leading-edge modification is shown in figure 4 and the ordinates are listed in table I. The wing trailing-edge modification required the extension of the trailing edge at the wing root and this resulted in a gap between the trailing edge of the wing and the bottom of the fuselage. This gap was eliminated by a fairing. Details of the trailing-edge extension and the fairing are shown in figures 5 and 6, respectively. The addition of area to the rearward fuselage section was based on the transonic area rule (refs. 8 and 9). Details of the area addition (called the modified full area bump) are shown in figure 6. The cross-sectional area distribution of the basic model is shown in figure 7. Also shown are the effects of two of the modifications on the area distribution; the area distribution for the leading-edge modification was not available. The inlets were open during the test. The area distribution rearward of the inlet has been modified by deducting an area equal to inlet area multiplied by mass-flow ratio (0.75) to account for the internal flow.

The model was mounted on a six-component strain-gage balance that was in turn supported by a sting mounting system. Photographs of the model installed in the 8-foot transonic pressure tunnel, with all three modifications in place, are presented in figures 8(a) and 8(b). The weights of the various model components were as follows:

Component	Weight, lb
Fuselage and tail surfaces	69.0
Strain-gage balance	4.25
Wing, inside fuselage	6.1
Wing, outside fuselage:	
Basic	18.9
Basic + leading edge	19.0
Basic + leading edge + trailing edge . .	20.1

Shake tests were made to establish the natural frequencies of all vibration modes that seemed likely to appear in the test results. The frequencies determined with the model mounted in the tunnel are shown in the following table:

Mode	Natural frequency, cps
Rigid-body vertical translation (on sting) . .	7
Rigid-body pitching	14
Rigid-body rolling	$22\frac{1}{4}$
First wing mode	184
Second wing mode	240
Third wing mode	388

Shake tests of the various configurations showed that none of the modifications changed the first-mode natural frequency by more than 1 percent. The node lines for the first three wing modes are sketched in figure 9.

In connection with the type of buffet analysis that is used in reference 6, certain constants are required. For this model, these constants have the following values based on the mode shape used in reference 6:

F_S dimensionless structural factor, 0.052

k_S physical factor, 2,197 ft^2-$lb^{1/2}$

Instrumentation

The model lift was determined from the normal force and chord force indicated by a six-component electrical strain-gage balance that was mounted within the model. The lift coefficients are based on the area of the basic wing, 2.60 square feet. Through consideration of the static calibrations of the balance and repeatability of data, the lift coefficient is estimated to be accurate within ±0.007 for data taken at a stagnation pressure of 0.80 atmosphere and ±0.017 for data taken at a stagnation pressure of 0.33 atmosphere.

Angle of attack was determined with a pendulum-type strain-gage unit located in the model support strut. Corrections were made for sting and balance deflections under load. The estimated accuracy of the angle of attack is 0.1°.

A bending-moment strain-gage bridge was mounted in a recess at the 57.14-percent-chord location near the root of the left wing as shown in figures 3 and 8(b). Analysis of static load calibrations showed that

this bridge measured pure bending moment about an axis that intersects the longitudinal axis of the model at an angle of 28°. The bending-moment axis is shown in figure 3.

During the tests, the output of the bending-moment gage was recorded on magnetic tape. A record of about 45 seconds in duration was taken at each test point. The power spectral density was determined from the tape record by means of the equipment and procedure described in reference 10. The filter band width used in the analysis varied from 30 cps, for a broad picture of the overall spectrum, to $1\frac{1}{4}$ cps for detailed study of the spectrum in the vicinity of the natural frequency of the first mode of the wing.

Tests

Buffet tests were made at Mach numbers from 0.80 to 1.00, with an angle-of-attack range of approximately -4° to 9°. All configurations were tested at a tunnel stagnation pressure of 0.80 atmosphere. (Balance force limits prevented testing at higher pressure.) In order to determine the effect of density on the magnitude of the buffet bending moment, the basic configuration was also tested at a much lower stagnation pressure, 0.33 atmosphere. The Reynolds number ranges for the two stagnation pressures are shown in figure 10.

RESULTS AND DISCUSSION

The discussion starts with an examination of the frequency spectrum of the wing bending moment in order to learn which vibration modes are evident and which are significant. The effect of air density on the root-mean-square bending moment is then shown, and is followed by an extensive examination of the system damping coefficients. The results of this part of the analysis determined the process that was used to reduce the buffet data. The next section covers the buffet input force and the effect of the modifications on this force. The discussion closes with comments regarding the prediction of flight buffet loads from wind-tunnel tests.

Frequency Spectrum of Bending Moment

The power spectral density of the output of the bending-moment gage, as determined by electrical analysis with a filter band width of 30 cps, is plotted in figure 11 for a typical buffet condition. These results are for a lift coefficient beyond the buffet boundary at a Mach number

of 0.95. The most striking feature of this spectrum is the high concen-
tration of energy in a few narrow frequency bands. The indication is
that for the purposes of analysis the model and supporting structure
could be regarded as a system with only a few degrees of freedom.

Influence of support flexibility.- The low-frequency peak shown in
figure 11 was found to be present throughout the investigation. The
shake tests show the presence of three well-defined low-frequency modes
that are connected with the flexibility of the sting and the strain-gage
balance. In order to determine which of these modes was responsible for
the observed low-frequency response, the data for several test points were
analyzed with a 3-cps band width filter. Samples of these analyses are
shown in figure 12. Figure 12(a) shows data obtained at $\alpha = 0^\circ$ at a
Mach number of 0.95. Peaks are observed at frequencies that correspond
approximately to the natural frequencies of vertical translation and
rolling, respectively. The vertical translation response predominates.
Figure 12(b) shows similar results obtained during buffet $(\alpha = 4^\circ)$. Note
the change in scale. The same two modes are present, but in this case
the rolling response predominates. These results indicate that the buffet
excitation contains sizable antisymmetrical components even at low fre-
quencies. The spectral-density values in figure 12(b) are much higher
than those in figure 11 because of the increase in tunnel pressure and
the decrease in filter band width.

Because support flexibility is a factor that is not present in flight,
it is desirable to eliminate the effects of the low-frequency response in
the analysis of the wind-tunnel data. Two effects must be considered.
First, there is the direct contribution of the low-frequency response to
the wing stress. This contribution will be eliminated simply by disre-
garding the low-frequency part of the power spectrum in the analysis and
in the discussion that follows. Second, there is the possibility that
the low-frequency motion of the wing might change the flow over the wing
in such a manner that the buffet excitation at higher frequencies would
be affected. This effect is assumed to be negligible. In this connection,
a previous investigation (ref. 11) showed that oscillating an airfoil at
one frequency had negligible effect on the random air forces due to turbu-
lence and buffeting at higher frequencies under the conditions of that
experiment.

In buffet testing, it is highly desirable to have the support roll
frequency far removed from the first wing bending frequency. If this
condition cannot be satisfied, it is necessary to take steps to remove
the roll response from the output by other means, as for instance by
combining left- and right-wing gage outputs in such a way as to cancel
the antisymmetrical outputs.

Wing modes.- In addition to the low-frequency peak in the spectrum
shown in figure 11, which is to be neglected, there are several other

peaks. Most prominent is the peak in the vicinity of the wing first bending frequency. Smaller peaks are shown at frequencies corresponding to the natural frequencies of the second and third wing modes. The first mode obviously dominates the response of the wing in buffet. This result is in agreement with full-scale flight data (refs. 5 and 7) that show the predominant influence of the first mode for wings of various plan forms, including a $6\frac{1}{2}$ - percent-thick 60° triangular wing (ref. 7).

Because the power in the second and third wing modes is small compared with that in the first mode, a study of the large peak by itself should provide a good indication of the buffet characteristics of the wing. In the remainder of this paper, therefore, only the first-mode response of the wing is considered. The root-mean-square bending moments that are presented were determined by integration of the spectrum between limits of 150 and 210 cps.

Effect of Density on Root-Mean-Square Bending Moment

A change in the air density affects the magnitudes of both the force that excites the buffet vibration and the aerodynamic damping due to the motion of the wing. Flight tests at a constant Mach number and varying altitude have shown (refs. 6 and 7) that the net result is that the root-mean-square buffet stress is approximately proportional to the square root of the dynamic pressure. In these flights at constant Mach number, the velocity variation was much smaller than the density variation. Therefore, the results indicate that the bending stress is proportional to the square root of the density. Analytically, this result would be expected if the damping were predominantly aerodynamic, as was assumed in reference 7. In order to determine the effect of density on the buffet stresses of the wind-tunnel model, the basic configuration was tested at two different values of tunnel stagnation pressure. The results, for a Mach number of 0.80, are shown in figure 13 where the ratios σ_M/q and $\sigma_M/\sqrt{q}$ are plotted as functions of C_L. The velocities at the two stagnation pressures are identical; hence, q varies only because ρ varies. The results shown in figure 13 indicate, therefore, that the root-mean-square bending moment is more nearly proportional to ρ than to $\sqrt{\rho}$. Thus, the effect of air density on the buffet intensity is different for this model than for airplanes for which flight data are available. As a result, the equation presented in reference 7 (essentially, eq. (B14) with $g = 0$) cannot logically be used as a basis for the reduction and analysis of these data, nor can it be used to predict flight buffet loads from the data for this model. One of the basic assumptions underlying this buffet equation apparently has been violated in this test.

After observation of the preceding results, it was obvious that a new technique for data reduction was required. Before such a technique could be developed, however, it was necessary to determine the reason for the observed difference between flight and model results in the effect of density on the bending moment due to buffet. A study of the system damping coefficients proved most informative, and the results of this study are presented in some detail in the following section. The reader who is interested only in the buffet results of the present investigation may find them by turning to the section entitled "Buffet Input Force."

System Damping Coefficients

Determination of damping coefficients.- In the case of forced vibration of a single-degree-of-freedom linear system, it is possible to infer the value of the system damping from the shape of the response curve of the system. Two independent methods are available for this purpose and they are derived in appendix A. One method makes use of the relationship between the mean-square response and the peak response:

$$\gamma + \frac{g}{2} = \frac{1}{\pi} \frac{\overline{z_o^2}}{\Phi_{z_o}(\Omega_r)} \tag{1}$$

where $\overline{z_o^2}$ is the mean-square response and $\Phi_{z_o}(\Omega_r)$ is the peak response of the system. The other method uses the relationship between the band width at the half-power points and the frequency of resonance:

$$\gamma + \frac{g}{2} = \frac{1}{2} \Delta\Omega \tag{2}$$

where $\Delta\Omega$ is the difference between the frequency ratios at the two half-power points. The half-power points are those points on the spectrum at which the spectral density is exactly one-half as high as the spectral density at resonance (peak response). These two equations are given as equation (A12) and equation (A15) in appendix A. If, in an experimental investigation, the measured quantity were the wing bending moment, σ_M^2 would be inserted in equation (1) for the mean-square response and $\Phi_M(\Omega_r)$ would be inserted for the peak response.

Two assumptions are required to justify the use of these relationships in the analysis of buffet data. The first is the assumption that

the wing behaves like a single-degree-of-freedom system in the vicinity
of the natural frequency of the first symmetrical mode. The second
assumption is that the system input is independent of the frequency in
the range where the output is significant. For the buffeting model,
this frequency range is so narrow that the assumption will be substan-
tially satisfied by any reasonably smooth input spectrum, and therefore,
the asumption seems reasonable.

In either of the two methods for obtaining the damping coefficient,
it is essential that the band width of the filter that is used to obtain
the spectrum be considerably less than the band width of the system being
studied. The 30-cps band width used to obtain the spectrum shown in
figure 11 is much too large and, in fact, it proved necessary to use the
smallest available filter band width, about $1\frac{1}{4}$ cps, to obtain the damping
coefficients for this wing. A typical spectrum obtained by narrow-band-
width analysis is presented in figure 14. This spectrum was obtained
from the same data as the spectrum shown in figure 11. Comparison of
figures 11 and 14 shows that the wider band filter gives a peak value
that is far too low and a spectrum band width that is far too wide.

There are certain statistical problems encountered in making a
narrow-band analysis of the type shown in figure 14. For a fixed length
of record (in this case a 30-second loop of tape was analyzed), the con-
fidence that can be placed in the value obtained for any given point on
the spectrum will decrease as the filter band width decreases. Roughly
speaking, the problem is that as the filter band width is decreased, a
point is reached eventually where the mean value in the 30-second time
interval for this tiny segment of the frequency range may differ consid-
erably from the long-time mean value for this segment. The presence of
such errors is indicated by sharp erratic dips and peaks in the frequency
spectrum, some of which are evident in figure 14.

The effect of these errors on the accuracy of a damping-coefficient
determination must be considered. One method for determining the damping
coefficient is based on measurements of the peak response and the mean-
square response (eq. (1)). Only the peak response is affected by the
error under consideration. The other method requires the determination
of the band width at the half-power points (eq. (2)). The damping coeffi-
cient, as determined by this method, is affected by errors at the half-
power points and the peak. Both methods were used in the present analysis.
In the first method, it was necessary to modify the constant $1/\pi$ in
equation (1) to account for the fact that the mean-square values were
obtained by integrating only from 150 to 210 cps rather than from 0 to
∞ cps. This modification was accomplished by multiplying $1/\pi$ by the
ratio of the part of equation (A10b) in brackets to equation (A10a).
These equations are for $\gamma = 0$. The assumption of $\gamma = 0$ for the deter-
mination of this ratio causes negligible error, because the damping for

these tests was mostly structural, and it greatly facilitates the calculation. The modified equation that was obtained by this manipulation was solved graphically. In the second method (eq. 2), the response curves had to be smoothed in some instances in order to obtain a single-valued answer for the band width. The damping constants obtained by the first method have been plotted against those obtained by the second method in figure 15. The scatter is small except at the high damping values that were measured under nonbuffet (low-lift) test conditions. Thus, the statistical errors that are inherent in figure 14 do not interfere seriously with the determination of the system damping.

Figure 15 also permits a test of the assumption regarding the single-degree-of-freedom behavior of the buffeting wing. If equations (1) and (2) are equated, the result is a relationship that connects the band width, the peak response, and the mean-square response. If the output of the buffeting wing does not satisfy this relationship, then the assumption that the buffeting wing behaves like a linear, single-degree-of-freedom system with constant-spectral-density input is incorrect. The fact that the average of the data in figure 15 falls almost on the line of perfect agreement proves, however, that the experimental output does satisfy this relationship. The agreement is necessary, but not sufficient, to prove that the assumption is correct.

Effect of density.- In figure 16, damping coefficients are plotted as a function of C_L for tests of the same configuration at two different values of tunnel density. The corresponding values of dynamic pressure are given in the figure. The effect of a $2\frac{1}{2}$-fold increase in density is to decrease slightly the total system damping. The total damping is composed of two parts - aerodynamic damping and structural damping. Aerodynamic damping increases with increasing density; yet, in this experiment the total damping was found to decrease. Hence, the aerodynamic damping in this experiment is apparently much smaller than the structural damping.

Effect of lift.- Both sets of data in figure 16 show a large decrease in damping with increasing C_L. Because the aerodynamic damping is apparently small, the origin of the damping variation with C_L must be sought in the mechanical system of the model and supporting structure.

In this connection, it was observed that the damping at low values of C_L is considerably higher than would be expected for a solid aluminum wing. This observation led to a careful examination of the model in search of a possible source of sliding friction. The most likely source appears to be the dovetail joint by which the wing was attached to the fuselage. The supposition is that at low lift the joint is sufficiently

loose so that a bending vibration of the wing causes a slight relative
movement between the wing and fuselage portions of the joint and that
the damping is increased by the energy dissipation due to friction in
this joint. At high lift, the steady forces are supposed to result in
a tightening of this joint with a resultant decrease in the relative
movement due to vibration and, therefore, in the damping. If this is the
case, there should be a better correlation between the actual lift and
the damping than between C_L and the damping.

In order to test this supposition, two additional plots were made.
For the first plot, the damping coefficients for the basic configuration
that were determined with $0 < C_L < 0.15$ were averaged with the use of
data at all Mach numbers. Similar averages were formed for other inter-
vals of 0.15 in C_L. The data at the two different tunnel pressures were
treated separately. The results are shown plotted against C_L in fig-
ure 17(a). As was the case at $M = 0.80$, the increase in tunnel pressure
resulted in a decrease in damping.

For the second plot, a similar averaging procedure was used, with
lift intervals of 100 pounds for the low-pressure data and 250 pounds
for the high-pressure data. The results are shown plotted against lift
in figure 17(b). There is a much better correlation between the damping
and the lift than between the damping and C_L. This experimental result
is in accord with the supposed action of the wing-fuselage joint.

As a result of this investigation, it has become apparent that care
should be exercised in the design of buffet models to minimize the struc-
tural damping and to eliminate any variation of the structural damping
during wind-tunnel tests.

Buffet Input Force

Determination of input force.- The fact that the damping varied
considerably during the test means that the wing bending moment is not a
direct measure of the magnitude of the buffet forces that excite the wing
vibration, because the bending moment is a function of the damping as
well as of the exciting forces. Thus, in order to determine the effect
of the modifications on the buffet forces, it is necessary first to elimi-
nate the effect of variations in damping. The equations that govern the
response of a wing in buffeting have been presented in reference 7 for
the case where the wing is treated as a simple beam.

In appendix B, corresponding equations are derived for the more gen-
eral case of a platelike wing, the structural characteristics of which
are described by flexibility-influence-coefficient and mass matrices.

Unfortunately, the present wing was no longer available at the time it became clear that the influence of damping variations would have to be removed from the data, so the influence coefficients could not be determined and it was necessary to rely on the simple-beam analysis. Although the accuracy of results derived by representing the wing of this test as a simple beam may be open to question, the comparisons between the various configurations are not affected by either the beam assumption or the choice of mode shape.

For wings that can be treated as simple beams, a strain-gage installation on the wing can be calibrated in terms of the bending moment carried by a cross section of the wing, and a relationship between input force, damping, and bending-moment output can be derived. The equation for the spectral density of the generalized normal-force coefficient is

$$\Phi_{C_{N,1}}\left(\frac{\omega_1 c_{av}}{V}\right) = \frac{V}{c_{av}} \frac{\sigma_M^2}{M_{m,1}^2} \frac{M_1^2}{q^2 S_1^2} \frac{4\left(\gamma + \frac{g}{2}\right)}{\pi\omega_1} \tag{3}$$

This equation is obtained by combining equations (B12) and (B13), which are derived in appendix B. This equation has been used in the reduction of the data from the present investigation. The factor π was modified, as previously explained, to account for the fact that σ_M^2 is obtained by integration from 150 to 210 cps instead of 0 to ∞ cps. The assumed mode shape was the same as in reference 6.

The square root of the spectral density of the generalized normal-force coefficient is plotted as a function of C_L in figure 18 at Mach numbers from 0.80 to 1.00. The spectral density of the generalized normal-force coefficient at the first-mode natural frequency ω_1,

$$\Phi_{C_{N,1}}\left(\frac{\omega_1 c_{av}}{V}\right)$$

is the quantity that is fundamental to the generalized harmonic analysis. Under the assumptions made in the present analysis, however, the root-mean-square bending moment in the wing is directly proportional to the square root of this spectral density. The results are presented, therefore, in terms of the square root, which is denoted by

$$\left[\Phi_{C_{N,1}}\left(\frac{\omega_1 c_{av}}{V}\right)\right]^{1/2}$$

Basic configuration.- The results for the basic configuration
(fig. 18) are given by the circular symbols. Flagged circles indicate
data obtained at a tunnel stagnation pressure of 0.33 atmosphere. The
solid lines plotted in figure 18 were obtained by fairing straight-line
segments through the data for the basic configuration. The sharp break
(discontinuity in slope) defines the buffet boundary, as determined from
the wind-tunnel tests. The value of C_L at the buffet boundary decreases
from nearly 0.5 at $M = 0.80$ to about 0.15 at $M = 0.95$. As the Mach num-
ber increases above $M = 0.95$, the value of C_L at the buffet boundary
increases rapidly.

Effect of modifications.- The modifications were tested only at the
higher stagnation pressure (0.80 atmosphere). For this tunnel pressure,
the angle-of-attack range was limited by the internal strain-gage balance
so that data were obtained beyond the buffet boundary of the basic config-
uration only at Mach numbers from 0.90 to 0.95, where the buffet boundary
is lowest. The results for Mach numbers of 0.90, 0.925, and 0.95 show
that the buffet forces at the higher values of C_L were substantially
reduced by the modifications. At $M = 0.925$, for instance, the buffet
forces were reduced by the addition of the cambered leading edge. Adding
the swept trailing-edge extension resulted in a further reduction in the
buffet intensity. Adding the body bump had no appreciable effect at this
speed, but the data for $M = 0.95$ show a reduction in buffet intensity due
to the bump. Inasmuch as changes in body shape are known to affect both
the strength and the progression of the main flow shock over the wing,
this is a reasonable result. In general, it would seem that modifications
that improve the flow over the wing would reduce the buffet intensity.

The results are less conclusive with regard to the effects of the
modifications on the buffet boundary. The data for the fully modified
configuration at $M = 0.95$, for instance, seem open to either of two pos-
sible interpretations: (1) the buffet boundary is essentially unchanged
by the modifications, but the buffet forces have became particularly mild,
or (2) the buffet boundary has been moved out to a C_L beyond the range
of the test. In either event, the effect of the modification is favorable.

Effect of turbulence.- It is typical of figure 18 that at a given
Mach number the exciting force at low values of C_L is approximately con-
stant independent of both C_L and the modifications. This excitation is
believed to be due to wind-tunnel turbulence. Experience has shown that
if the turbulence level is too high, the location of the buffet boundary
tends to become obscured. From the nature of the power spectrum (fig. 11)
it is obvious that the important factor is not the overall turbulence
level in the tunnel, but rather the turbulence level at frequencies in the
vicinity of the wing natural frequency f_1. In the present tests the

root-mean-square value of the lateral component of turbulence in the frequency interval from 180 to 190 cps is estimated at less than 0.02° on the basis of turbulence surveys of the tunnel.

<p align="center">Comments Regarding Prediction of Flight</p>

<p align="center">Buffet Loads From Wind-Tunnel Tests</p>

If $C_{N,1}\left(\dfrac{\omega_1 c_{av}}{V}\right)$ and $C_{L_\alpha,1}$ are known, either from experimental results or theory, the root-mean-square amplitude of vibration can be calculated from the following equation which was obtained by substituting the appropriate values for $\Phi_N(\omega_1)$ and γ in equation (B9):

$$\sigma_{r_1} = \left[\frac{\Phi_{C_{N,1}}\left(\dfrac{\omega_1 c_{av}}{V}\right)}{\dfrac{C_{L_\alpha,1} q S_2}{2 M_1 \omega_1 V} + \dfrac{g}{2}}\right]^{\frac{1}{2}} \sqrt{\frac{\pi}{4}\frac{\omega_1 c_{av}}{V}} \frac{q S_1}{M_1 \omega_1^2} \tag{4}$$

In deriving the equation for the root-mean-square bending moment that is presented in reference 7, it was assumed that the structural damping is so small that it can be neglected in comparison with the aerodynamic damping. The corresponding equation for the vibration amplitude is obtained by setting $g = 0$ in equation (4)

$$\sigma_{r_1} = \left[\frac{\Phi_{C_{N,1}}\left(\dfrac{\omega_1 c_{av}}{V}\right)}{C_{L_\alpha,1}}\right]^{\frac{1}{2}} \sqrt{q} \left[\frac{\pi}{2}\frac{c_{av}}{\omega_1^2}\frac{S_1^2}{M_1 S_2}\right]^{\frac{1}{2}} \tag{5}$$

Available flight data support the assumption that the ratio of structural to aerodynamic damping is sufficiently small so that the structural damping can be neglected in buffet calculations (refs. 6 and 7). The results of the present investigation, however, show that this is not necessarily true for wind-tunnel models. (See the section of this paper entitled "System Damping Coefficients.")

There is a general tendency for the aerodynamic damping ratio γ of solid-metal model wings to be considerably lower than for airplane wings because of the higher density of the model wings. If, as in the present test, the values of q and V approximate the flight values, the aerodynamic damping will be proportional to the value of the constant $S_2/M_1\omega_1$

for the model and for the airplane. For the Douglas D-558-II, this con-
stant has the value 0.00858 for the 1/16-scale model described in ref-
erence 12 and 0.0646 for the full-scale airplane. Thus, the aerodynamic
damping ratio for the model is only about one-eighth of that for the
airplane. Because of this tendency toward much lower aerodynamic damping
ratios, the structural damping assumes a greater relative importance for
models than for airplanes. Thus, it would seem advisable in the design
of models to be used in buffet tests to try to minimize the structural
damping.

With regard to the results of the present investigation, any attempt
to predict flight vibration amplitudes or stresses must be based on an
estimate of $C_{L_\alpha,1}$ for the airplane. Unfortunately, there seem to be
no experimental data for swept wings on which to base this estimate.
Experimental aerodynamic damping ratios for two unswept wings are pre-
sented in reference 11.

CONCLUDING REMARKS

The buffet characteristics of a 1/10-scale model of an attack air-
plane have been investigated at Mach numbers from 0.80 to 1.00. The wing
had a modified delta plan form with an NACA 0008 (modified) airfoil sec-
tion at the root and an NACA 0005 (modified) airfoil section at the tip,
a leading-edge sweep of 41.11°, an aspect ratio of 2.91, and a taper
ratio of 0.226. Modifications to the basic configuration included a
tapered wing-leading-edge extension with camber, an addition to the wing
trailing edge sweeping it forward 10°, and an area addition to the rear-
ward fuselage section. In the speed range where the buffet boundary of
the basic configuration was lowest, the buffet intensity was reduced
substantially when these modifications were added to the model.

During buffet, the wing vibrated primarily in the first symmetrical
mode. The damping of the vibration was not primarily aerodynamic, as is
the case for airplanes in flight at these speeds, but instead was mostly
structural, apparently because of friction in a dovetail joint. As a
result, any attempt to predict flight buffet stresses from the results
of this investigation must be based on an estimate of the aerodynamic
damping for the airplane.

For the mathematical model of the buffeting wing there is a relation-
ship that connects the band width, the peak response, and the mean-square
response. The experimental results show that this same relationship holds
for the actual buffeting wing.

In designing buffet models, it is desirable to keep the structural damping very low because the aerodynamic damping ratio is much lower for solid-metal model wings than for actual airplane wings.

Langley Aeronautical Laboratory,
    National Advisory Committee for Aeronautics,
        Langley Field, Va., July 31, 1957.

APPENDIX A

DERIVATION OF EQUATIONS RELATING DAMPING CONSTANT AND

POWER SPECTRUM OF SYSTEM RESPONSE

Consider a linear single-degree-of-freedom system with aerodynamic damping and structural damping both present. The equation of motion for such a system, in a steady-state forced vibration, can be written (combine eqs. (3.25) and (3.68), ref. 13):

$$\ddot{z} + 2\omega_n\gamma\dot{z} + \omega_n^2(1 + ig)z = \frac{F_o}{m} e^{i\omega t} \tag{A1}$$

where ω_n is the undamped natural frequency and γ is the aerodynamic damping ratio. If a solution of the form $z = z_o e^{i(\omega t-\beta)}$ is assumed, the vibration amplitude z_o is found to be given by the following equation:

$$z_o = \frac{\dfrac{F_o}{m\omega_n^2}}{\sqrt{\left(1 - \dfrac{\omega^2}{\omega_n^2}\right)^2 + \left(2\gamma\dfrac{\omega}{\omega_n} + g\right)^2}} \tag{A2}$$

With the substitution $\Omega = \dfrac{\omega}{\omega_n}$ this becomes

$$z_o = \frac{\dfrac{F_o}{m\omega_n^2}}{\sqrt{\left(1 - \Omega^2\right)^2 + \left(2\gamma\Omega + g\right)^2}} \tag{A3}$$

The frequency of maximum response is termed the resonant frequency (Ω_r or ω_r). This frequency can be found by maximizing equation (A3). The exact result is

$$\Omega_r = \sqrt{1 - 2\gamma^2 - \frac{\gamma g}{\Omega_r}} \tag{A4}$$

which can be solved easily by iteration. An approximation that is
entirely adequate for lightly damped systems, for which Ω_r is nearly 1,
is

$$\Omega_r \approx \sqrt{1 - 2\gamma^2 - \gamma g} \qquad (A5)$$

This equation is exact for $\gamma = 0$ or for $g = 0$. When the damping is
30 percent of critical (with $\gamma = 0.15$, $g/2 = 0.15$), the error is about
1/10 of 1 percent.

According to the principles of generalized harmonic analysis, if
the system is excited by a random force with spectral density $\Phi_{F_o}(\Omega)$,
then the spectral density of the displacement is

$$\Phi_{z_o}(\Omega) = \Phi_{F_o}(\Omega) \left| A(\Omega) \right|^2$$

where $\left| A(\Omega) \right|^2$ is the square of the absolute value of the system admit-
tance. (This input-output relationship is given in reference 4 in terms
of the impedance, which is the reciprocal of the admittance.) From equa-
tion (A3)

$$\left| A(\Omega) \right|^2 = \frac{\dfrac{1}{m^2 \omega_n^4}}{\left(1 - \Omega^2\right)^2 + (2\gamma\Omega + g)^2}$$

and, therefore,

$$\Phi_{z_o}(\Omega) = \frac{\dfrac{\Phi_{F_o}(\Omega)}{m^2 \omega_n^4}}{\left(1 - \Omega^2\right)^2 + (2\gamma\Omega + g)^2} \qquad (A6)$$

When equation (A4) is substituted into equation (A6), the spectral
density of the displacement at the resonant frequency is found to be

$$\Phi_{z_o}(\Omega_r) = \frac{\dfrac{\Phi_{F_o}(\Omega_r)}{m^2 \omega_n^4}}{(2\gamma + g)^2 - \gamma^2\left(4\gamma^2 + 4\gamma g + g^2\right) + o\left(\gamma^6\right)}$$

For lightly damped systems this is approximately

$$\Phi_{z_O}(\Omega_r) = \frac{\dfrac{\Phi_{F_O}(\Omega_r)}{m^2\omega_n{}^4}}{4\left(\gamma + \dfrac{g}{2}\right)^2} \tag{A7}$$

The integrated mean-square response of the system is given by

$$\overline{z_O{}^2} = \int_0^\infty \frac{\dfrac{\Phi_{F_O}(\Omega)}{m^2\omega_n{}^4}}{\left(1 - \Omega^2\right)^2 + (2\gamma\Omega + g)^2}$$

or, for the special case where the spectral density of the exciting force $\Phi_{F_O}(\Omega)$ is a constant independent of frequency

$$\overline{z_O{}^2} = \frac{\Phi_{F_O}(\Omega)}{m^2\omega_n{}^4} \int_0^\infty \frac{d\Omega}{\left(1 - \Omega^2\right)^2 + (2\gamma\Omega + g)^2} \tag{A8}$$

If either g or γ is zero, the integral in equation (A8) can be evaluated in closed form. For $g = 0$,

$$\int_{\Omega_A}^{\Omega_B} \frac{d\Omega}{\left(1 - \Omega^2\right)^2 + (2\gamma\Omega)^2} = \left[\frac{1}{8\sqrt{1 - \gamma^2}} \log_e \frac{r_1}{r_2} + \frac{1}{4\gamma} \tan^{-1} \frac{2\Omega\gamma}{1 - \Omega^2}\right]_{\Omega_A}^{\Omega_B} \tag{A9a}$$

where

$$r_1 = 1 + \Omega^2 + 2\Omega\sqrt{1 - \gamma^2}$$

$$r_2 = 1 + \Omega^2 - 2\Omega\sqrt{1 - \gamma^2}$$

When the integral of equation (A9a) is evaluted for the limits $\Omega_A = 0$ and $\Omega_B = \infty$ and the result is substituted into equation (A8), the

following equation is obtained:

$$\overline{z_o{}^2} = \frac{\Phi_{F_o}(\Omega)}{m^2\omega_n{}^4} \frac{\pi}{4\gamma} \tag{A9b}$$

For $\gamma = 0$:

$$\int_{\Omega_A}^{\Omega_B} \frac{d\Omega}{\left(1 - \Omega^2\right)^2 + g^2} = \frac{1}{2\sqrt{2}\ g\sqrt{1 + g^2}} \left[\sqrt{\sqrt{1 + g^2} - 1}\ \log_e \frac{r_1}{r_2} - \right.$$

$$\left. \sqrt{\sqrt{1 + g^2} + 1}\ \tan^{-1} r_3 \right]_{\Omega_A}^{\Omega_B} \tag{A10a}$$

where

$$r_1 = \left[\Omega^2 + 2\sqrt{2}\ \Omega\sqrt{\sqrt{1 + g^2} + 1} + \sqrt{1 + g^2} \right]^{1/2}$$

$$r_2 = \left[\Omega^2 - 2\sqrt{2}\ \Omega\sqrt{\sqrt{1 + g^2} + 1} + \sqrt{1 + g^2} \right]^{1/2}$$

$$r_3 = \frac{\sqrt{2}\ \Omega\sqrt{\sqrt{1 + g^2} - 1}}{\Omega^2 - \sqrt{1 + g^2}}$$

When the integral of equation (A10a) is evaluated for the limits $\Omega_A = 0$ and $\Omega_B = \infty$ and the result is substituted into equation (A8), the following equation is obtained:

$$\overline{z_o{}^2} = \frac{\Phi_{F_o}(\Omega)}{m^2\omega_n{}^4} \left[\frac{\pi}{2g} \frac{\sqrt{\frac{1}{2} + \frac{1}{2}\sqrt{1 + g^2}}}{\sqrt{1 + g^2}} \right] \tag{A10b}$$

For the case where the system damping is low, a satisfactory approximation to equation (A8) is

$$\overline{z_o{}^2} = \frac{\Phi_{F_o}(\Omega)}{m^2\omega_n{}^4}\frac{\pi}{4\left(\gamma + \frac{g}{2}\right)} \tag{A11}$$

This result has been obtained for the special case $\Phi_{F_o}(\Omega) = $ Constant.

The error of the approximation in equation (A11) has been determined for three combinations of γ and $g/2$, each with a total damping ratio of 0.04, with the following results:

γ	$g/2$	Error in eq. (A11), percent
0.04	0	0
.02	.02	.11
0	.04	.024

For the special case of a lightly damped system with constant density excitation, equations (A7) and (A11) can be combined to yield a relationship between the damping, the mean-square response, and the peak response:

$$\gamma + \frac{g}{2} = \frac{1}{\pi}\frac{\overline{z_o{}^2}}{\Phi_{z_o}(\Omega_r)} \tag{A12}$$

In case the mean square value is obtained from an integration over a limited range rather than from 0 to ∞, this equation can be modified as explained in the discussion of figure 15 in the section of the paper entitled "System Damping Coefficients."

A second equation for the damping can be derived independently from the frequencies at the half-power points on the response curve. These frequencies can be determined by finding the maximum value of the integrand in equation (A8) and then solving for the frequencies at which the value of the integrand is exactly one-half of the maximum value. This has been done for the two special cases $g = 0$ and $\gamma = 0$. For $g = 0$:

$$\Omega_{1/2} = \left[1 - 2\gamma^2 \pm 2\gamma\sqrt{1 - \gamma^2}\right]^{1/2} \tag{A13a}$$

The two solutions given by this equation yield the difference $\Delta\Omega$ between the upper and lower half-power points. The solution for γ in terms of

this difference is

$$\gamma = \frac{1}{\sqrt{2}}\left[1 + \frac{1}{2}(\Delta\Omega)^2 - \sqrt{1 + \frac{1}{2}(\Delta\Omega)^4}\right]^{1/2} \qquad \text{(A13b)}$$

For $\gamma = 0$:

$$\Omega_{1/2} = \sqrt{1 \pm g} \qquad \text{(A14a)}$$

and

$$g = \Delta\Omega\sqrt{1 - \frac{1}{4}(\Delta\Omega)^2} \qquad \text{(A14b)}$$

For combined viscous and structural damping, a suitable approximation for lightly damped systems is

$$\gamma + \frac{g}{2} = \frac{1}{2}\Delta\Omega \qquad \text{(A15)}$$

The error in equation (A15) has been determined for three combinations of γ and $g/2$, each with a total damping ratio of 0.04, with the following results:

γ	$g/2$	Error in eq. (A15), percent
0.04	0	1.965
.02	.02	.165
0	.04	.080

APPENDIX B

DERIVATION OF EQUATIONS GOVERNING BUFFET

RESPONSE OF A WING

In deriving the buffet equations the procedure will be to determine the normal modes of the wing, to set up the equation for a steady-state forced vibration by Lagrange's method, to solve this equation in order to determine the admittance of the vibrating system, and then to apply the methods of generalized harmonic analysis to determine the response of the system to a random (buffet) input.

The normal modes of vibration can be determined from the structural characteristics of the wing as described by certain matrices (ref. 13, 14, or 15). For analysis, the wing is divided into a suitable group of elements, each of which is associated with a particular point in the plane of the wing. The elastic properties of the wing are contained in a square matrix of flexibility-influence coefficients, which can be determined by analysis of the structure or by direct measurement. If $\{P\}$ is a set of static loads and $\{z\}$ is a corresponding set of displacements, then

$$\{z\} = [A]\{P\}$$

where $[A]$ is the matrix of flexibility-influence coefficients. The inertial properties of the wing are described by a diagonal matrix, each element of which is the mass associated with an element of the wing. This matrix is denoted by $[M]$. The matrix $[U] = [A][M]$ is called the dynamic matrix.

The matrix equation

$$\{z\} = \omega^2[U]\{z\}$$

is solved to obtain the frequencies and shapes of the normal modes of vibration (ref. 13, p. 169). The frequency of the nth mode will be written ω_n and the column matrix containing the associated normalized set of deflections will be written $\{\varphi^{(n)}\}$.

The displacement of the mth element of the vibrating wing can be written in terms of a series utilizing the normal modes:

$$z_m = \sum_n r_n \varphi_m{}^{(n)}$$

where the terms r_n are functions of time. The kinetic energy of the vibrating system is then (ref. 13, p. 45)

$$T = \frac{1}{2} \sum_n M_n \dot{r}_n{}^2$$

where

$$M_n = \sum_m m_m \left(\varphi_m{}^{(n)} \right)^2$$

and the terms m_m are the elements of the inertia matrix $\left[M \right]$. The elastic strain energy V is (refs. 13 and 14)

$$V = \frac{1}{2} \sum_n \omega_n{}^2 M_n r_n{}^2$$

These expressions for the kinetic and potential energies, when inserted in Lagrange's equation, yielded the equation of motion for the nth mode:

$$M_n \ddot{r}_n + \omega_n{}^2 M_n r_n = \sum_m P_m \varphi_m{}^{(n)} \qquad \text{(B1)}$$

where P_m represents the forces, other than inertial and elastic, that act on the element m.

The results of this test and others (refs. 5 and 7) have shown that, in many instances of wing buffet, most of the energy in the power spectrum of buffet bending moment is concentrated at frequencies in the vicinity of the natural frequency of the first mode. Normally the first mode is well separated from the higher modes, and as a result the response of the higher modes at the first mode frequency is very small. Attention can

be confined, therefore, to a study of the first mode. The set of equations (B1) then reduces to the single equation

$$M_1 \ddot{r}_1 + \omega_1{}^2 M_1 r_1 = \sum_m P_m \varphi_m{}^{(1)} \tag{B2}$$

One of the forces that contribute to P_m is the pressure fluctuation that causes the buffet; this pressure fluctuation is called the exciting force. The force on element m is $\Delta p_m s_m$ and the corresponding generalized force on the wing is

$$N_1 = \sum_m \Delta p_m s_m \varphi_m{}^{(1)}$$

It is convenient to define what might be termed a generalized normal-force coefficient for the first mode:

$$C_{N,1} = \frac{N_1}{q S_1} \tag{B3}$$

where

$$S_1 = \sum_m s_m \varphi_m{}^{(1)} \tag{B4}$$

Another force that contributes to P_m is the aerodynamic force due to the motion of the wing. For simple harmonic motion, this force for an element m of the wing is of the form

$$a_m \ddot{r}_1 + b_m \dot{r}_1 + c_m r_1$$

with the corresponding generalized force being

$$\ddot{r}_1 \sum_m a_m \varphi_m{}^{(1)} + \dot{r}_1 \sum_m b_m \varphi_m{}^{(1)} + r_1 \sum_m c_m \varphi_m{}^{(1)}$$

In this simplified treatment of the buffet phenomena, the first and last terms of this generalized force are assumed to be negligible in comparison

with $M_1\ddot{r}_1$ and $\omega_1{}^2M_1r_1$, respectively. Further consideration is given to the second term, which arises from the aerodynamic forces that oppose the vertical velocity of each element m. The resulting pressure difference has the form

$$\Delta p_m = -qk_m\, \frac{\dot{z}_m}{V} = -q\, \frac{k_m}{V}\, \dot{r}_1\varphi_m{}^{(1)}$$

where $\dot{z}_m/V$ is an effective angle of attack and k_m is a constant of the nature of a local lift-curve slope that depends on the plan form and mode shape. The minus sign signifies that the pressure opposes the motion. The corresponding generalized force is

$$-L_1\dot{r}_1 = -q\, \frac{\dot{r}_1}{V} \sum_m k_m s_m\left(\varphi_m{}^{(1)}\right)^2$$

It is convenient to define what might be called a generalized lift-curve slope for the first mode:

$$C_{L_{\alpha,1}} = \frac{\displaystyle\sum_m k_m s_m\left(\varphi_m{}^{(1)}\right)^2}{S_2} \tag{B5}$$

where

$$S_2 = \sum_m s_m\left(\varphi_m{}^{(1)}\right)^2 \tag{B6}$$

so that

$$L_1\dot{r}_1 = C_{L_{\alpha,1}}\, \frac{\dot{r}_1}{V}\, qS_2 \tag{B7}$$

The equation of motion can now be written as

$$M_1\ddot{r}_1 + L_1\dot{r}_1 + \omega_1{}^2M_1r_1 = N_1$$

The term $L_1\dot{r}_1$ is the generalized aerodynamic damping force. Structural damping can be included in the equation by adding a term $ig\omega_1{}^2M_1r_1$ (ref. 13, p. 197). For a sinusoidal exciting force $N_1 = N \sin \omega t$ the equation of motion is then

$$M_1\ddot{r}_1 + L_1\dot{r}_1 + (1 + ig)\omega_1{}^2M_1r_1 = N \sin \omega t$$

which is of the same form as equation (A1). The steady-state solution of this equation is

$$r_1 = \frac{N}{M_1\omega_1{}^2} \frac{\sin (\omega t - \beta)}{\sqrt{\left(1 - \frac{\omega^2}{\omega_1{}^2}\right)^2 + \left(2\gamma \frac{\omega}{\omega_1} + g\right)^2}}$$

where $\gamma = \dfrac{L_1}{2M_1\omega_1}$ and β is the phase angle by which the displacement lags the force. For use in the generalized harmonic analysis of buffeting, the square of the absolute value of the admittance is required:

$$|A(\omega)|^2 = \frac{1}{M_1{}^2\omega_1{}^4\left[\left(1 - \frac{\omega^2}{\omega_1{}^2}\right)^2 + \left(2\gamma \frac{\omega}{\omega_1} + g\right)^2\right]} \tag{B8}$$

According to the principles of generalized harmonic analysis the response of this system to a random input $\Phi_N(\omega)$ is

$$\Phi_{r_1}(\omega) = \Phi_N(\omega)|A(\omega)|^2$$

The mean-square value is given by

$$\overline{r_1{}^2} = \int_0^\infty \Phi_N(\omega)|A(\omega)|^2 d\omega$$

In the case of a lightly damped system, the response is concentrated in a narrow frequency band near ω_1. In that band the response is very

nearly

$$\Phi_{r_1}(\omega) = \Phi_N(\omega_1)|A(\omega)|^2$$

if the input spectrum is reasonably smooth. Flight-test results (ref. 7) show that all but a very small part of the response power for a buffeting wing is found in the frequency band near ω_1 and, therefore, the mean-square response will be very nearly

$$\overline{r_1^2} = \Phi_N(\omega_1) \int_0^\infty |A(\omega)|^2 d\omega$$

Approximating the integral as in equation (A11) gives

$$\overline{r_1^2} \approx \Phi_N(\omega_1) \frac{\pi\omega_1}{M_1^2\omega_1^4 4\left(\gamma + \frac{g}{2}\right)} \tag{B9}$$

Assume now that a strain gage has been mounted on the wing at any point that experiences strain fluctuations during first-mode vibration of the wing. When the wing vibrates in the first mode, the elongation sensed by the gage and hence the gage output, will be directly proportional to the amplitude r_1 of the vibration. Hence, r_1 can be determined with a properly calibrated strain gage. (The case where the wing is vibrating in several modes is not considered herein. Such a case involves solution of the set of equations (B1) rather than of a single equation of the set.) Thus the power spectrum $\Phi_{r_1}(\omega)$ and the mean-square value $\overline{r_1^2}$ of the vibration amplitude can be obtained from analysis of the strain-gage output.

The value of the damping $\gamma + g/2$ can be determined from an analysis of the strain-gage output by either of the two methods described in appendix A. With the damping and the mean-square response known, equation (B9) can be solved for the spectral density of the exciting force:

$$\Phi_N(\omega_1) = \overline{r_1^2} \frac{M_1^2\omega_1^4 4\left(\gamma + \frac{g}{2}\right)}{\pi\omega_1} \tag{B10}$$

This result can be converted to coefficient form by means of the power-spectrum equivalent of equation (B3), that is,

$$\Phi_{C_{N,1}}(\omega) = \frac{\Phi_{N_1}(\omega)}{q^2 S_1^2}$$

with the following result:

$$\Phi_{C_{N,1}}(\omega_1) = \overline{r_1^2} \omega_1^4 \frac{M_1^2}{q^2 S_1^2} \frac{4\left(\gamma + \frac{g}{2}\right)}{\pi \omega_1} \tag{B11}$$

In the case where a wing can be treated as a simple beam, the strain gages can be calibrated in terms of the beam bending moment, and a relationship can be derived between the bending moment and the generalized input force for first-mode bending of the wing. This is the procedure followed in reference 7. The equation for the spectral density of the generalized normal-force coefficient is (compare with eq. (B11))

$$\Phi_{C_{N,1}}(\omega_1) = \frac{\sigma_M^2}{M_{m,1}^2} \frac{M_1^2}{q^2 S_1^2} \frac{4\left(\gamma + \frac{g}{2}\right)}{\pi \omega_1} \tag{B12}$$

where σ_M^2 is the mean-square bending moment. The constants M_1, $M_{m,1}$, and S_1 are as defined in reference 7. Because the wing is considered as a continuous beam, the generalized masses and areas are obtained by integration rather than by summations such as equation (B4).

The results of the present investigation are presented in terms of the nondimensional frequency parameter $\frac{\omega_1 c_{av}}{V}$ by use of the transformation

$$\Phi_{C_{N,1}}\left(\frac{\omega_1 c_{av}}{V}\right) = \frac{V}{c_{av}} \Phi_{C_{N,1}}(\omega_1) \tag{B13}$$

The use of this parameter was suggested in reference 16.

The equation for the root-mean-square bending moment as a function of $\Phi_{C_{N,1}}\left(\dfrac{\omega_1 c_{av}}{V}\right)$ is

$$\sigma_M = 2k_S F_S \frac{\sqrt{q}}{\sqrt{1 + \dfrac{g}{2\gamma}}} \left[\frac{\Phi_{C_{N,1}}\left(\dfrac{\omega_1 c_{av}}{V}\right)}{C_{L_{\alpha,1}}}\right]^{1/2} \tag{B14}$$

The derivation of this equation is essentially the same as that of equation (1) in reference 6, except that structural damping g has been included in this case. Equation (B14) also differs from equation (8) in reference 7 (same as eq. (1), ref. 6) by a factor of 2 that was inadvertently omitted in the derivation of that equation. Thus the values of the quantities symbolized by

$$\left[\frac{C_N\left(\dfrac{\omega_1 \bar{c}}{V}\right)}{C_{L_\alpha}\left(\dfrac{\omega_1 \bar{c}}{V}\right)}\right]^{1/2}$$

and

$$\Phi\left(\frac{\omega_1 \bar{c}}{V}\right) = \left\{\frac{\partial}{\partial \Delta C_N}\left[\frac{C_N\left(\dfrac{\omega_1 \bar{c}}{V}\right)}{C_{L_\alpha}\left(\dfrac{\omega_1 \bar{c}}{V}\right)}\right]^{1/2}\right\}$$

as presented in references 6 and 7 are exactly twice as large as the values that would be obtained by the use of equation (B14). Because the references use the same equation consistently, the values of σ_M are not affected by the omission of this constant factor.

For the limiting case $\gamma = 0$, the root-mean-square bending moment is, from equations (B12) and (B13),

$$\sigma_M = \frac{S_1 M_{m,1}}{M_1}\sqrt{\frac{\pi}{2g}}\sqrt{\frac{\omega_1 c_{av}}{V}}\, q\left[\Phi_{C_{N,1}}\left(\frac{\omega_1 c_{av}}{V}\right)\right]^{1/2} \tag{B15}$$

Thus for $\gamma = 0$, $\sigma_M \propto q \propto \rho$; while for $g = 0$, $\sigma_M \propto \sqrt{q} \propto \sqrt{\rho}$ (eq. (B14)).

REFERENCES

1. Gadeberg, Burnett L., and Ziff, Howard L.: Flight-Determined Buffet
   Boundaries of Ten Airplanes and Comparisons With Five Buffeting
   Criteria. NACA RM A50I27, 1951.

2. Kantor, M.: Estimation of the Buffet-Onset Boundary for Straight and
   Swept-Wing Airplanes. Tech. Memo. 1-53, Aero. and Hydro. Branch,
   Bur. Aero., Mar. 20, 1953.

3. Martin, Andrew, and Reed, James F.: Correlation of Buffet Boundaries
   Predicted From Wind-Tunnel Tests With Those Measured During Flight
   Tests on the F8F-1 and X-1 Airplanes - Transonic-Bump Method. NACA
   RM A52J17, 1952.

4. Liepmann, H. W.: On the Application of Statistical Concepts to the
   Buffeting Problem. Jour. Aero. Sci., vol. 19, no. 12, Dec. 1952,
   pp. 793-800, 822.

5. Huston, Wilber B., and Skopinski, Ted H.: Probability and Frequency
   Characteristics of Some Flight Buffet Loads. NACA TN 3733, 1956.

6. Skopinski, T. H., and Huston, Wilber B.: A Semiempirical Procedure
   for Estimating Wing Buffet Loads in the Transonic Region. NACA
   RM L56E01, 1956.

7. Huston, Wilber B., Rainey, A. Gerald, and Baker, Thomas F.: A Study
   of the Correlation Between Flight and Wind-Tunnel Buffeting Loads.
   NACA RM L55E16b, 1955.

8. Whitcomb, Richard T.: A Study of the Zero-Lift Drag-Rise Character-
   istics of Wing-Body Combinations Near the Speed of Sound. NACA
   Rep. 1273, 1956. (Supersedes NACA RM L52H08.)

9. Holdaway, George H.: Comparison of Theoretical and Experimental Zero-
   Lift Drag-Rise Characteristics of Wing-Body-Tail Combinations Near
   the Speed of Sound. NACA RM A53H17, 1953.

10. Smith, Francis B.: Analog Equipment for Processing Randomly Fluctu-
    ating Data. Aero. Eng. Rev., vol. 14, no. 5, May 1955, pp. 113-119.

11. Rainey, A. Gerald.: Measurement of Aerodynamic Forces for Various
    Mean Angles of Attack on an Airfoil Oscillating in Pitch and on Two
    Finite-Span Wings Oscillating in Bending With Emphasis on Damping
    in the Stall. NACA TN 3643, 1956.

12. Kemp, William B., Jr., and King, Thomas, J., Jr.: Wind-Tunnel Meas-
      urements of Wing Buffeting on 1/16-Scale Model of Douglas D-558-II
      Research Airplane. NACA RM L56G31, 1956.

13. Scanlan, Robert H., and Rosenbaum, Robert: Introduction to the Study
      of Aircraft Vibration and Flutter. The Macmillan Co., 1951.

14. Fung, Y. C.: An Introduction to the Theory of Aeroelasticity. GALCIT
      Aeronautical Series. John Wiley & Sons, Inc., c.1955.

15. Bisplinghoff, Raymond L., Ashley, Holt, and Halfman, Robert L.: Aero-
      elasticity. Addison-Wesley Pub. Co., Inc. (Cambridge, Mass.),
      c.1955.

16. Liepmann, H. W.: Parameters for Use in Buffet Flight Tests. Rep.
      No. SM-14631, Douglas Aircraft Co., Inc., Jan. 3, 1953.

TABLE I.- AIRFOIL ORDINATES FOR BASIC WING

AND LEADING-EDGE MODIFICATION[a]

Root-chord ordinates of modified NACA 0008, percent c			Tip-chord ordinates of modified NACA 0005, percent c			Modified leading-edge ordinates at 0.873b/2, percent c		
Station	Upper	Lower	Station	Upper	Lower	Station	Upper	Lower
0	0	0	0	0	0	-9.48	-2.65	-2.65
1.1	1.50	-----	1.2	.83	-----	-9.42	-2.39	-2.92
1.4	----	-1.14	1.3	----	-.47	-9.33	-2.25	-3.03
2.3	2.19	-----	2.4	1.22	-----	-9.18	-2.07	-3.13
2.7	----	-1.53	2.6	----	-.55	-8.75	-1.71	-3.32
4.8	3.15	-----	4.9	1.77	-----	-8.02	-1.31	-3.43
5.2	----	-2.00	5.1	----	-.61	-6.55	-.70	-3.41
7.3	3.80	-----	7.4	2.15	-----	-5.57	-.18	-3.32
7.7	----	-2.31	7.6	----	-.65	-3.61	.27	-3.18
9.9	4.25	-----	10.0	2.41	-----	-.66	1.01	-2.90
10.1	----	-2.54	10.1	----	-.71	2.27	1.59	-2.67
15.0	4.72	-2.88	15.0	2.73	-.90	5.20	2.09	-2.49
20.0	4.85	-3.08	20.0	2.89	-1.12	8.14	2.49	-2.37
25.0	4.83	-3.17	25.0	2.98	-1.33	11.07	2.80	-2.27
30.0	4.75	-3.20	30.0	3.05	-1.50	14.01	3.07	-2.24
40.0	4.46	-3.13	40.0	3.10	-1.78	16.96	3.22	-2.25
50.0	4.01	-2.90	50.0	3.05	-1.95	19.89	3.28	-2.35
60.0	3.41	-2.53	60.0	2.86	-1.98			
70.0	2.70	-2.04	70.0	2.47	-1.81			
80.0	1.89	-1.45	80.0	1.85	-----			
90.0	.99	-.77	90.0	1.04	-.82			
95.0	.52	-.41	95.0	.59	-.48			
100.0	0	0	100.0	0	0			
L.E. radius: 0.70 percent c			L.E. radius: 0.21 percent c					

[a]Stations and ordinates referenced to the leading edge and wing reference plane of the basic wing.
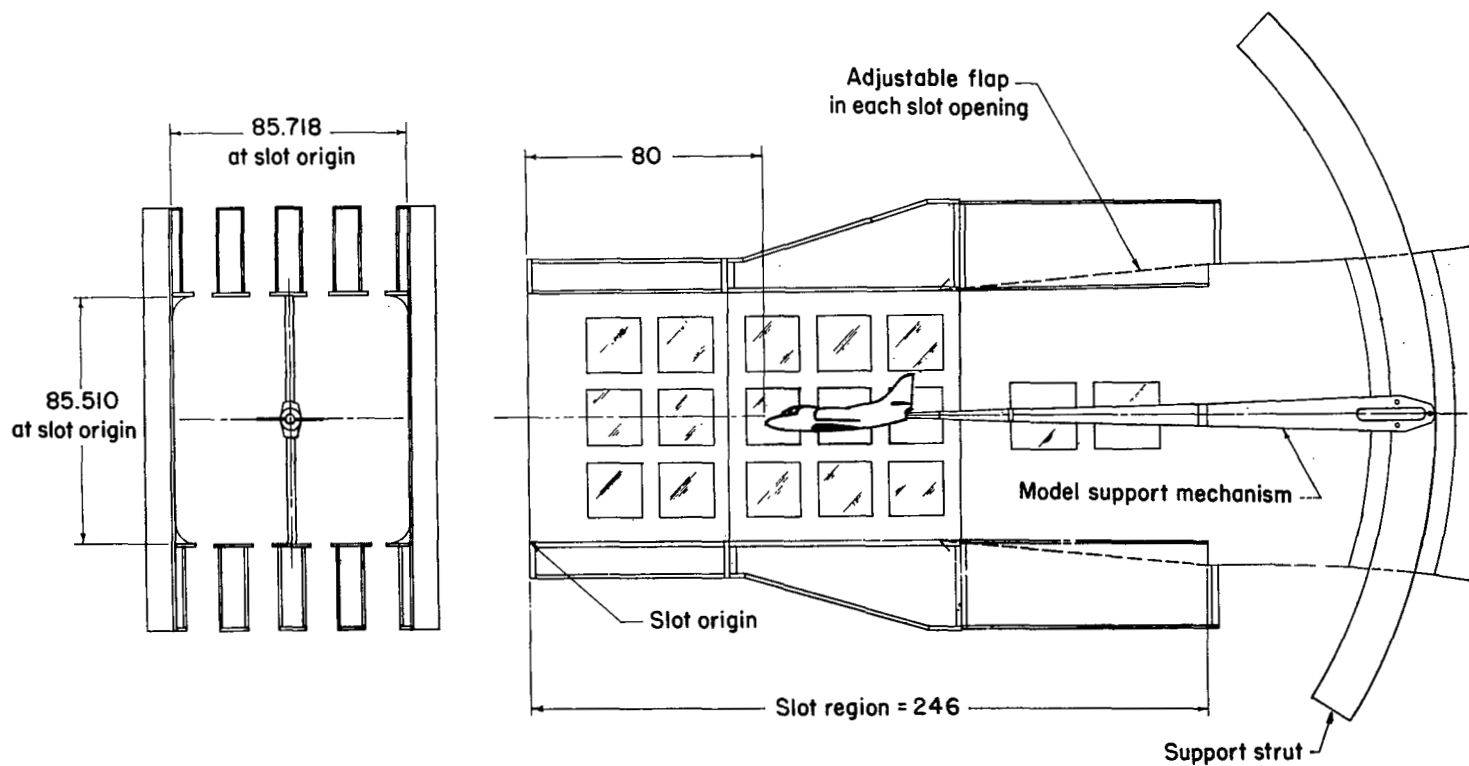
Figure 1.- Details of test section and location of model in the Langley 8-foot transonic pressure tunnel. All dimensions are in inches.
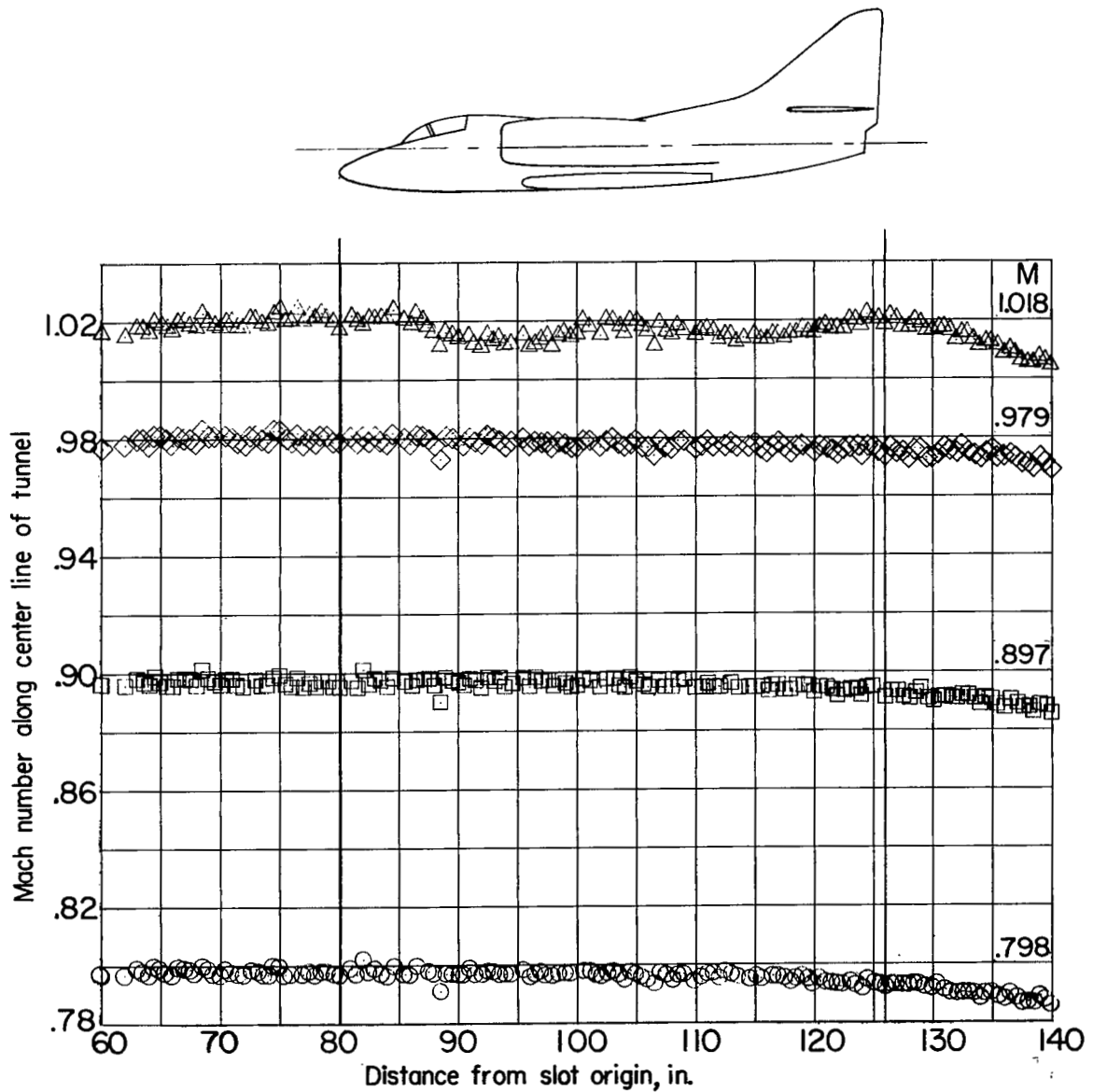
Figure 2.- Local Mach number distribution over the test section
occupied by the model. Atmospheric stagnation pressure.

WING GEOMETRY

Airfoil section (parallel to plane of symmetry)	
Root	NACA 0008 (modified)
Tip	NACA 0005 (modified)
Area, total, sq ft	2.60
Aspect ratio	2.91
Incidence, deg	0
Dihedral, deg	2.67

Figure 3.- Three-view drawing of the 0.10-scale model of the attack airplane. All dimensions are in inches unless otherwise noted.
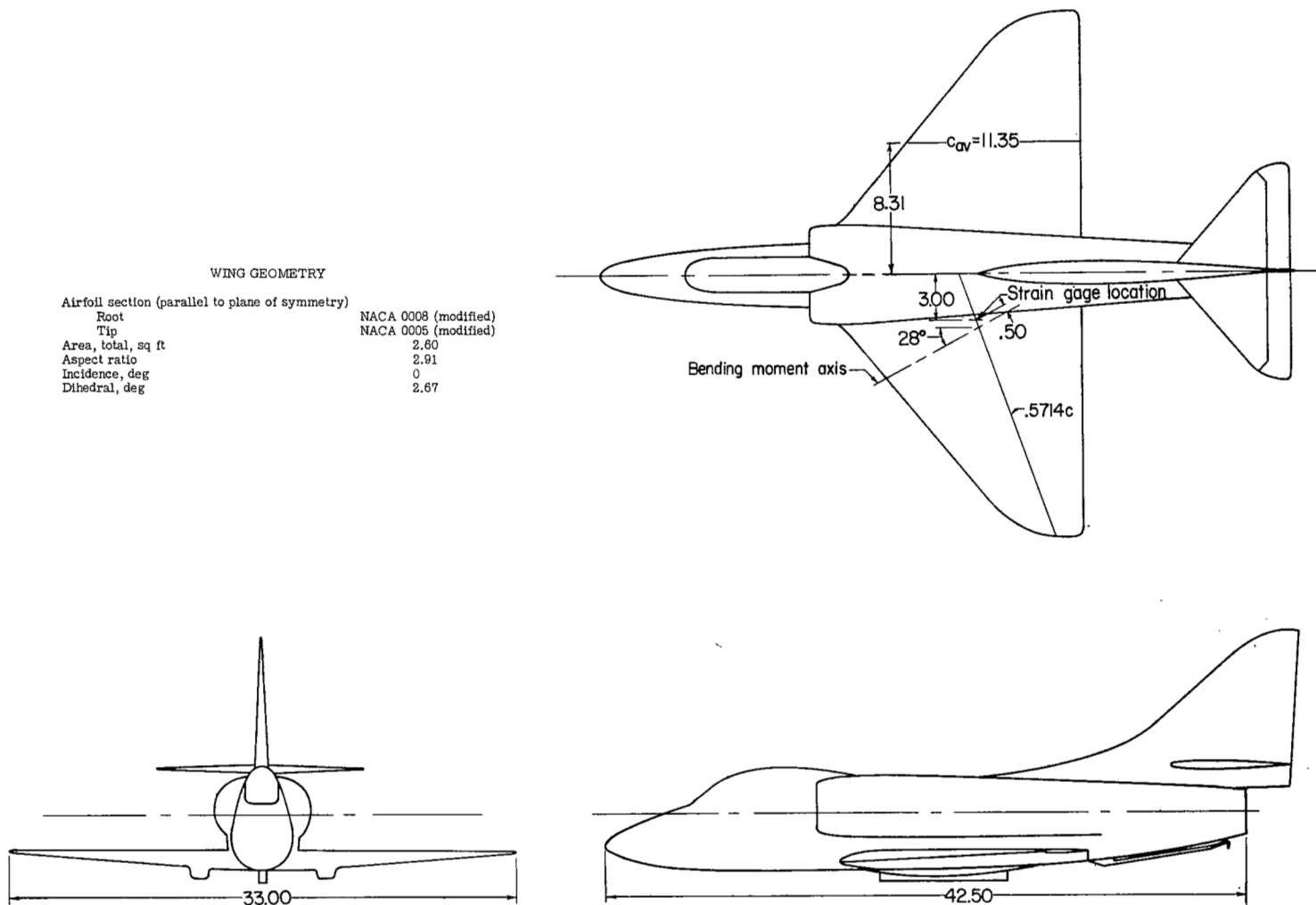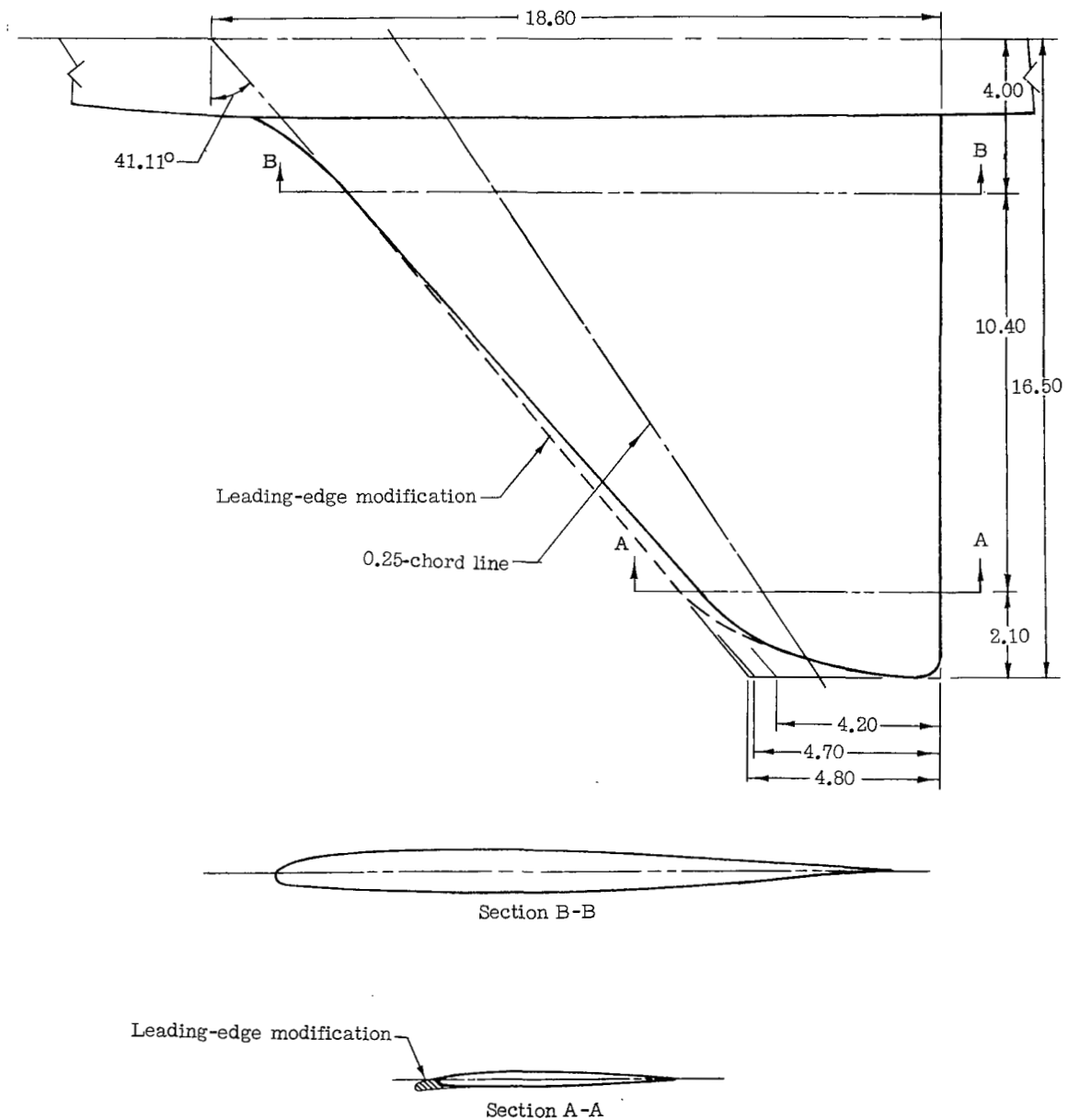
Figure 4.- Dimensional details of wing leading-edge modification. All
dimensions are in inches unless otherwise noted.
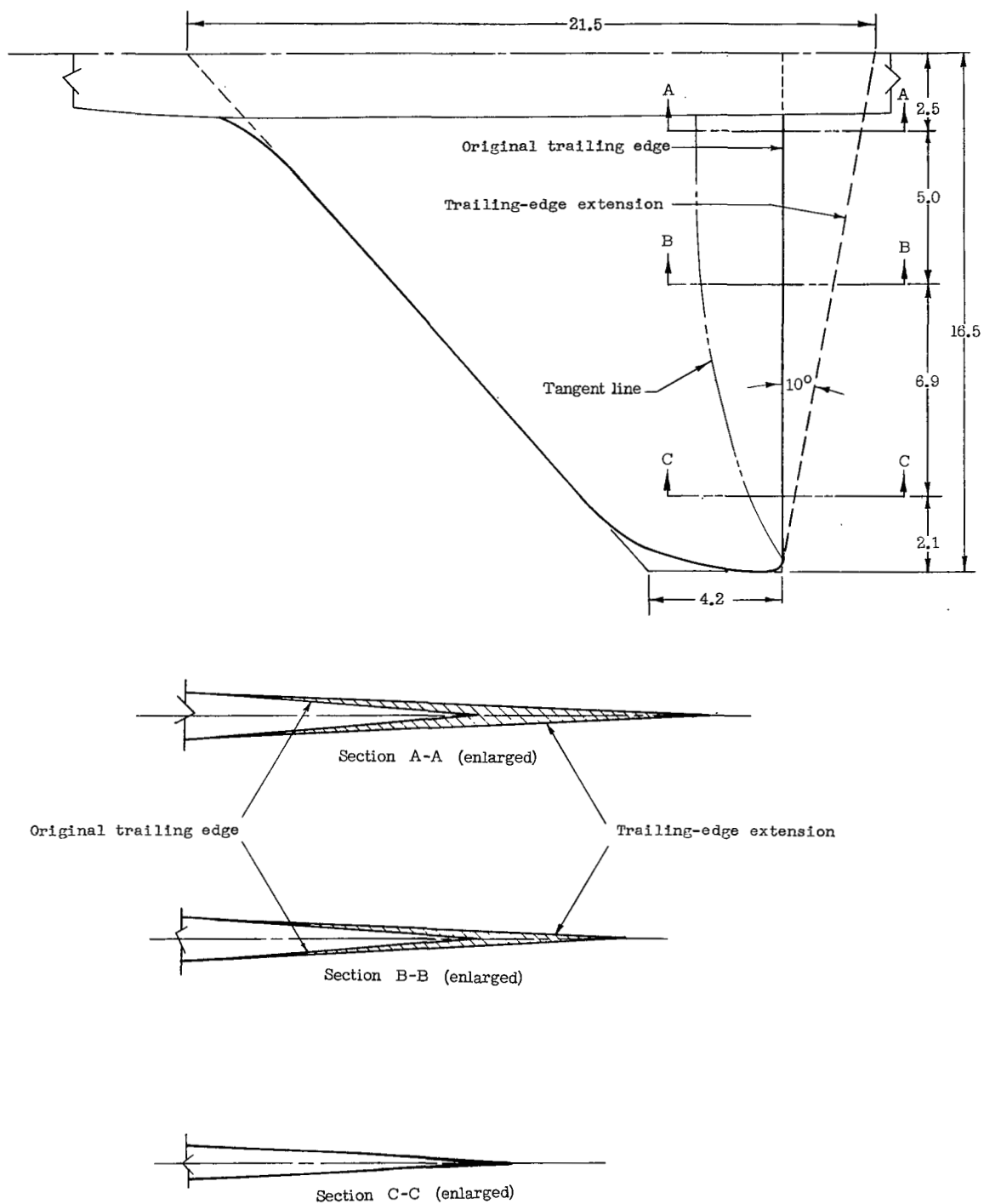
Figure 5.- Dimensional details of wing trailing-edge extension. All dimensions are in inches unless otherwise noted.
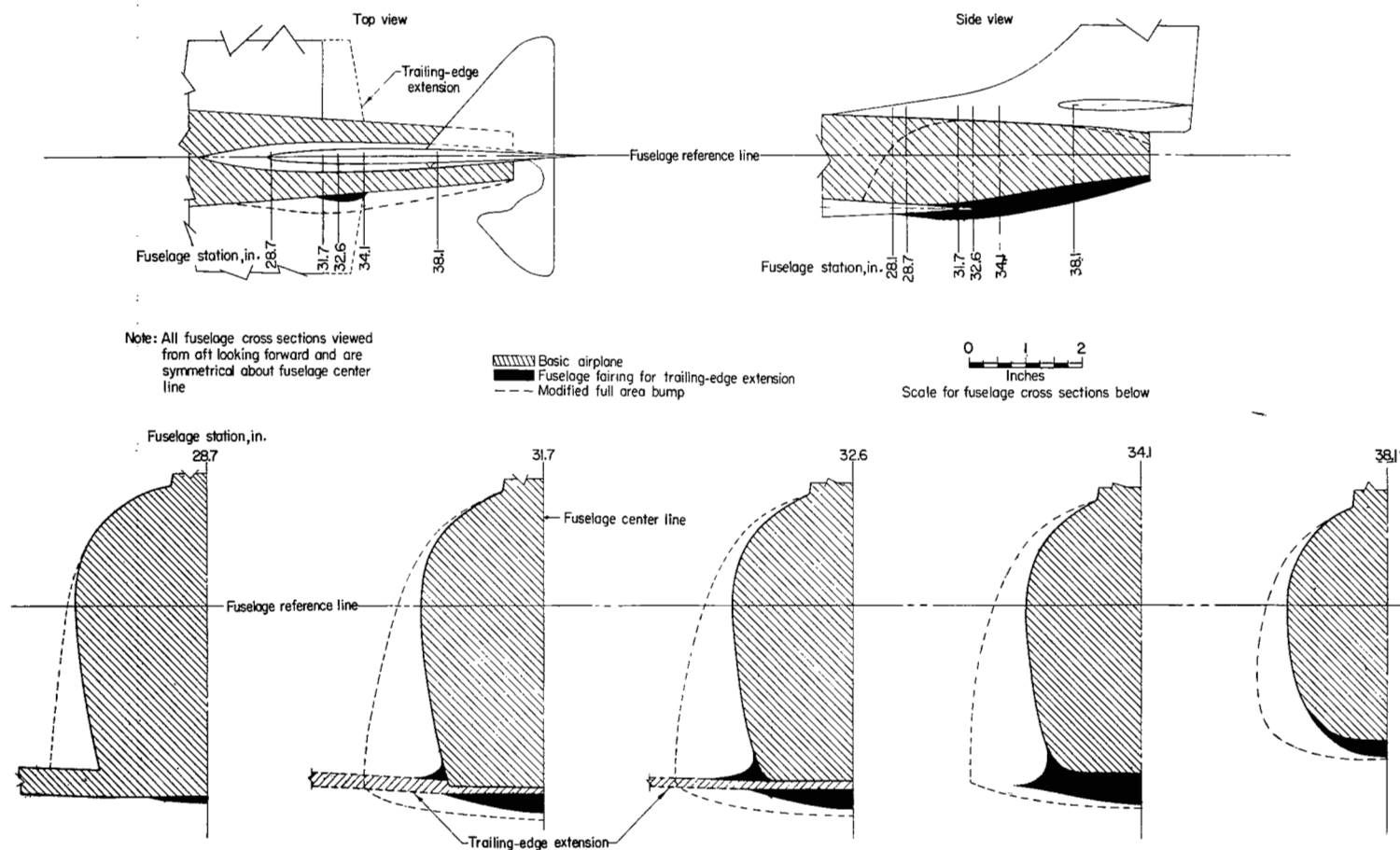
Figure 6.- Details of fuselage modifications.
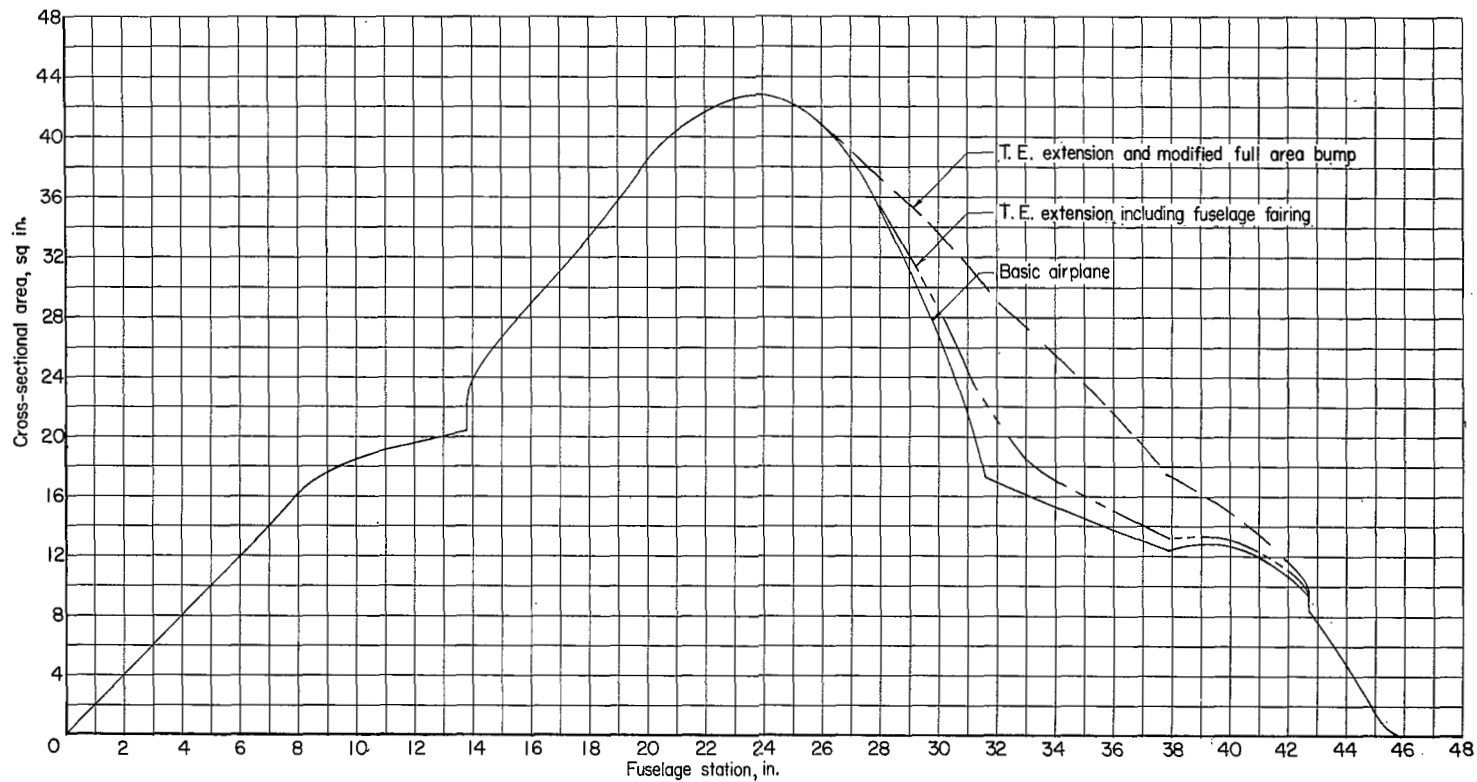
Figure 7.- Axial distributions of cross-sectional area for the 0.10-scale model of the attack airplane. Free-stream area required to pass inlet mass flow (3.56 square inches) removed rearward of duct inlet.
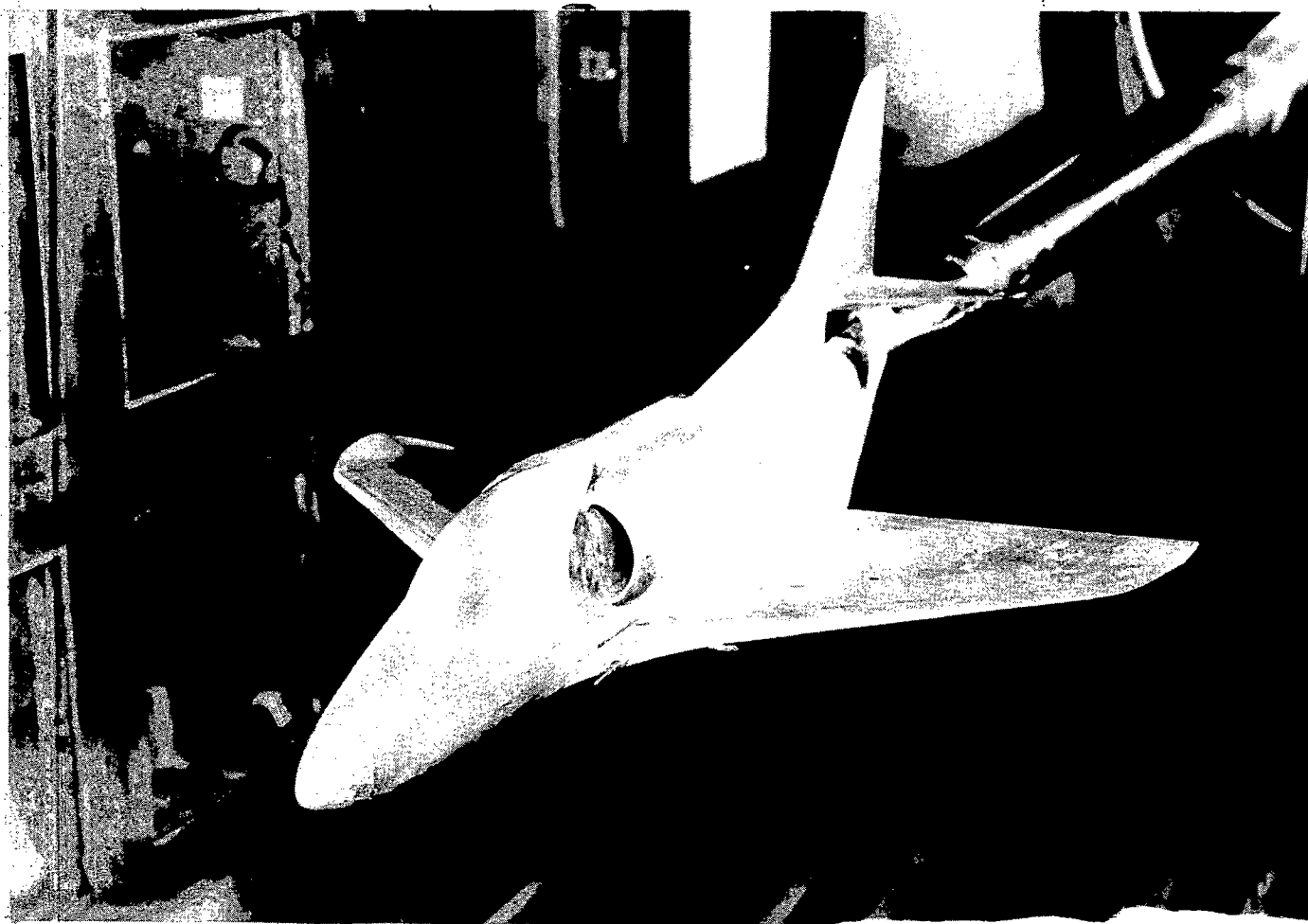
(a) Three-quarter front view.   L-89766

Figure 8.- Model installed in the Langley 8-foot transonic pressure tunnel. (Modifications to wing leading edge, wing trailing edge, and fuselage included.)
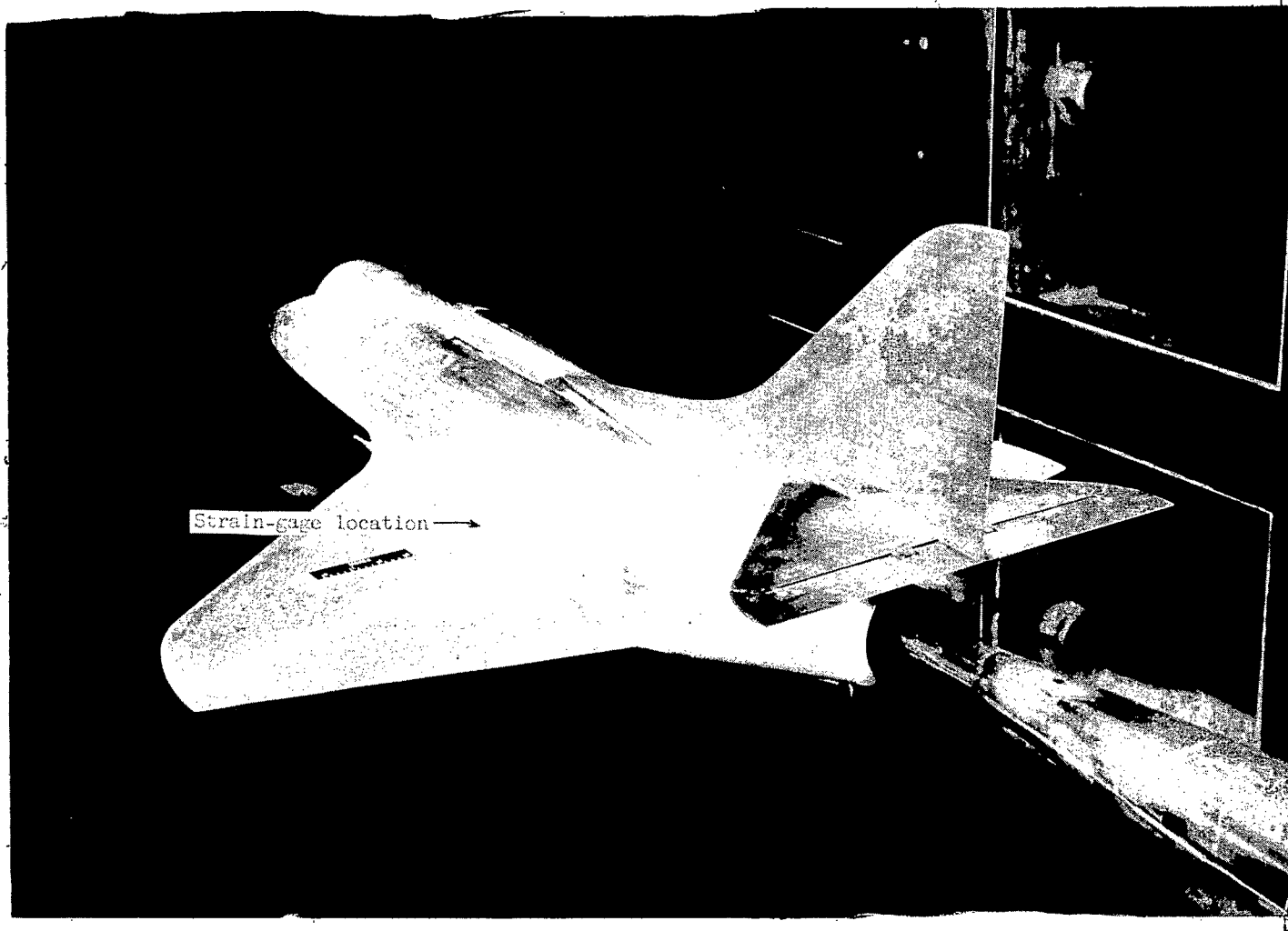
(b) Three-quarter rear view. L-90012.1

Figure 8.- Concluded.
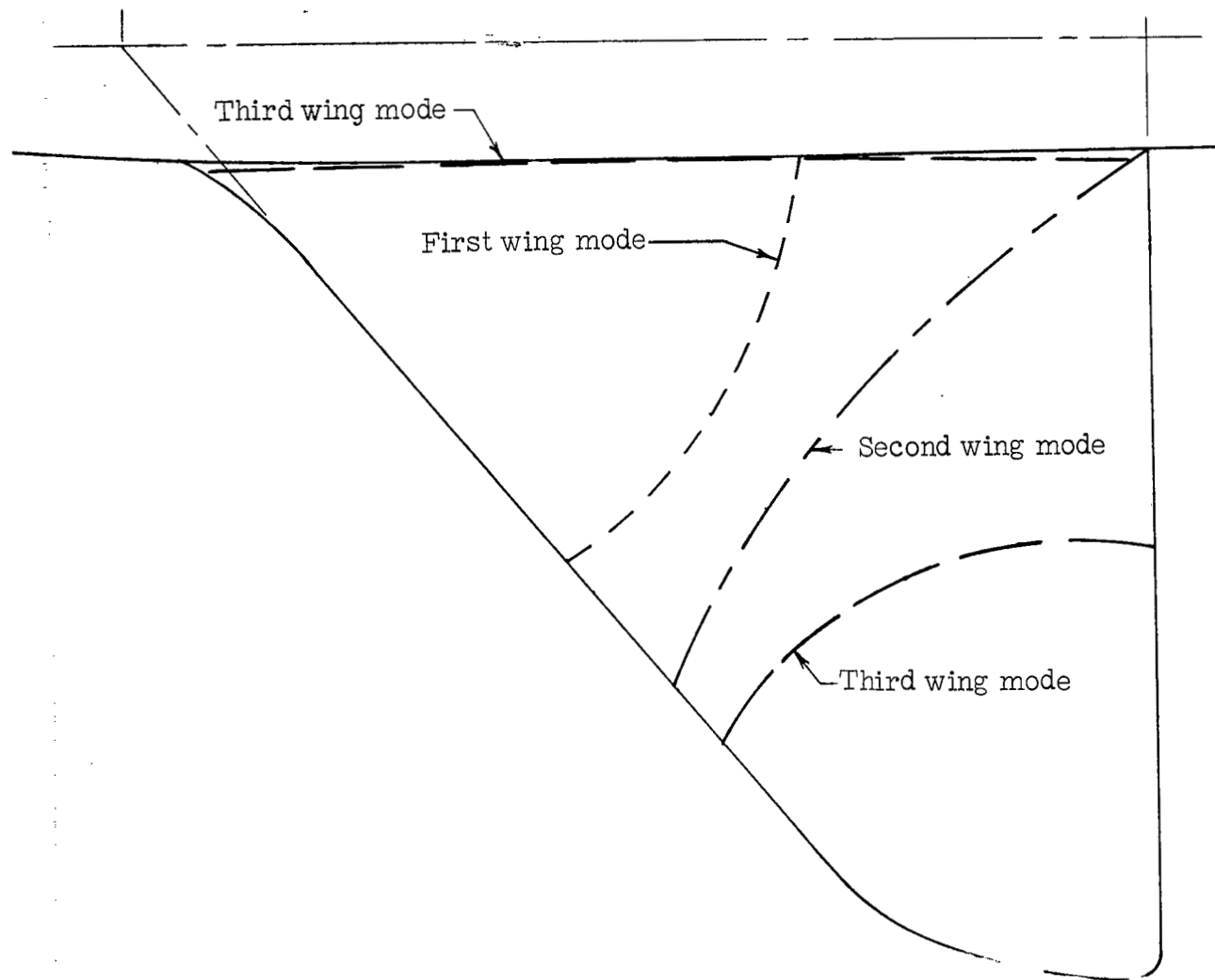
Figure 9.- Wing node lines for the first three wing modes obtained from shake tests.
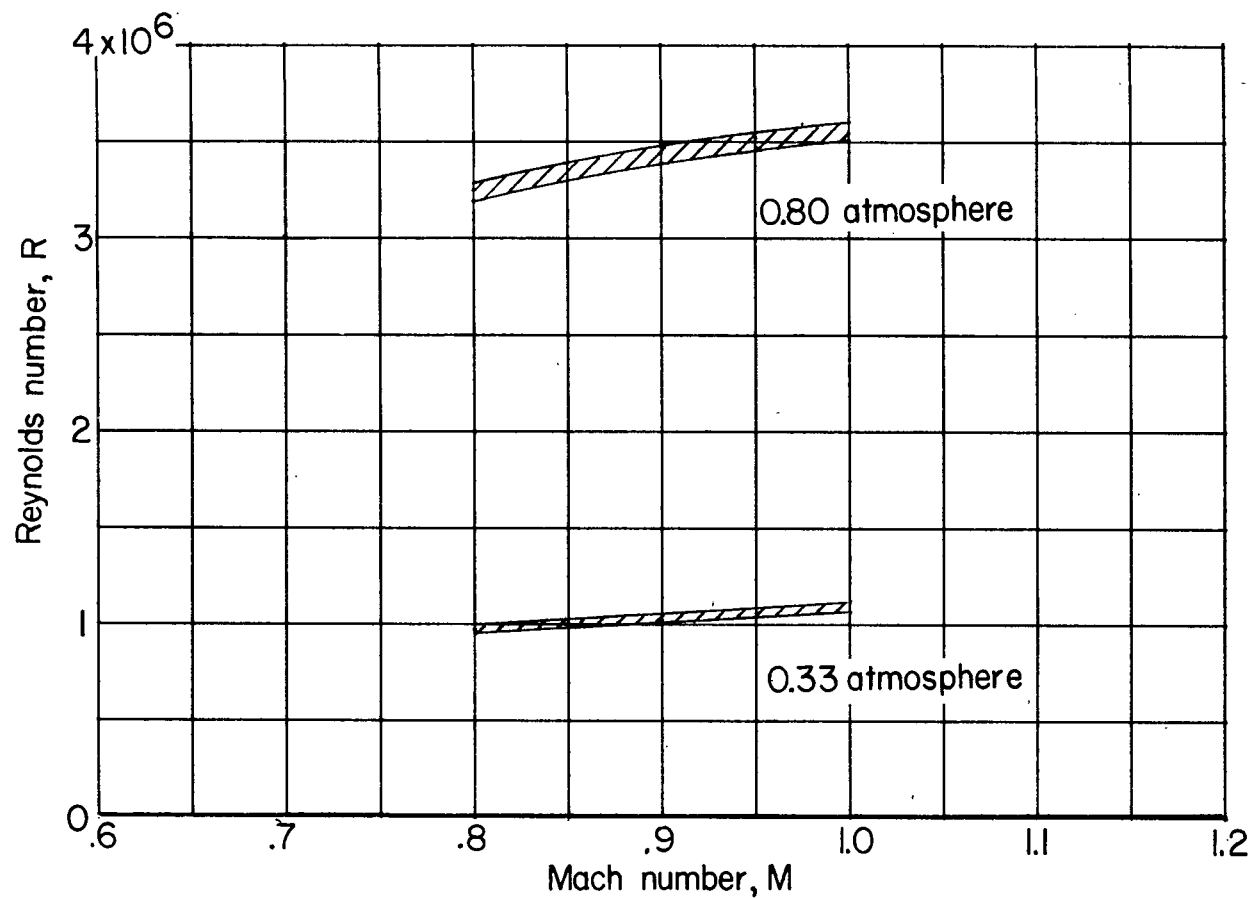
Figure 10.- Variation with Mach number of Reynolds number based on mean aerodynamic chord for the two stagnation pressures.
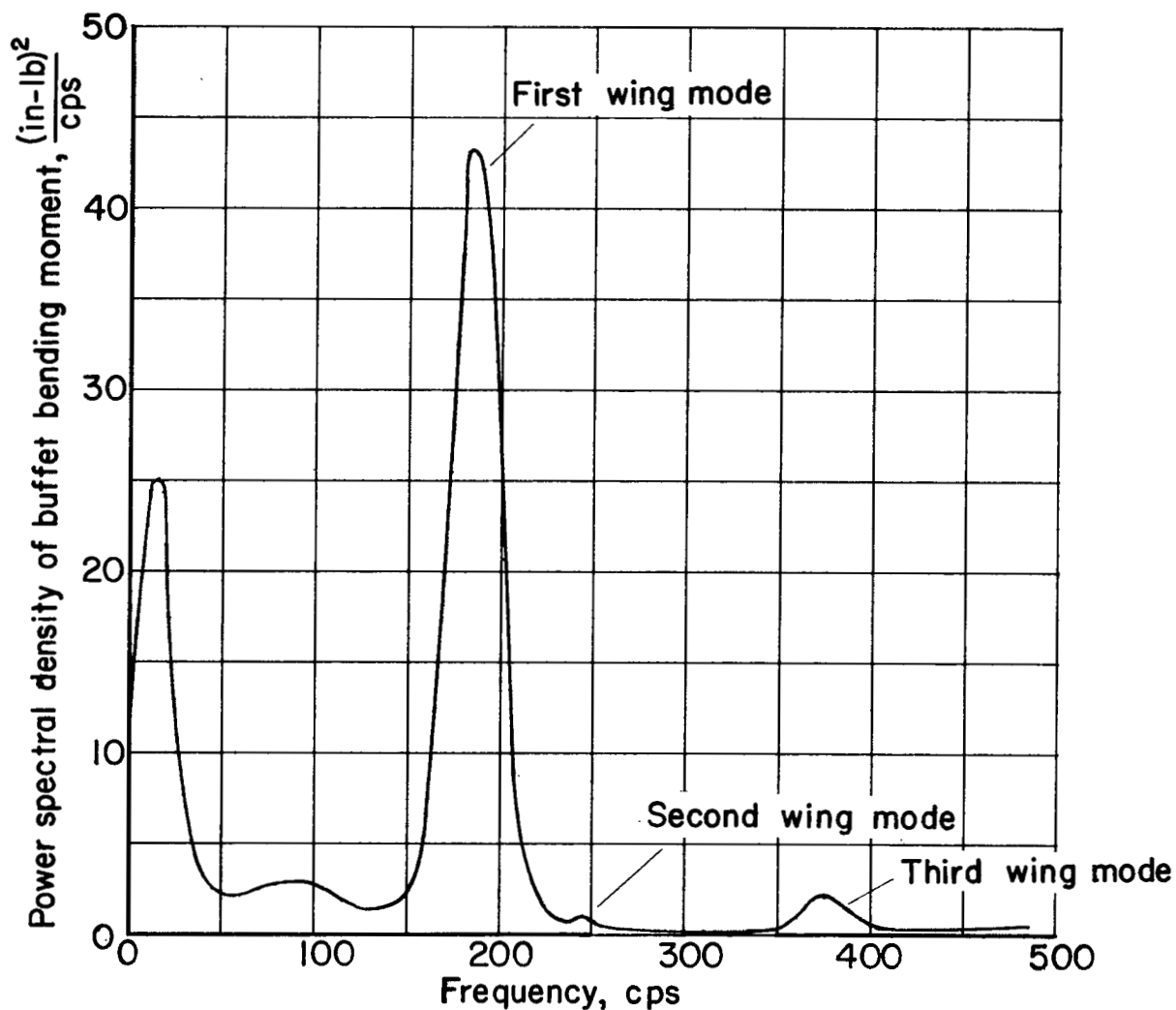
Figure 11.- Typical spectrum of the output of the bending-moment gage with a filter band width of 30 cycles per second. Basic model at 0.33 atmosphere for M = 0.95 and α = 6°.
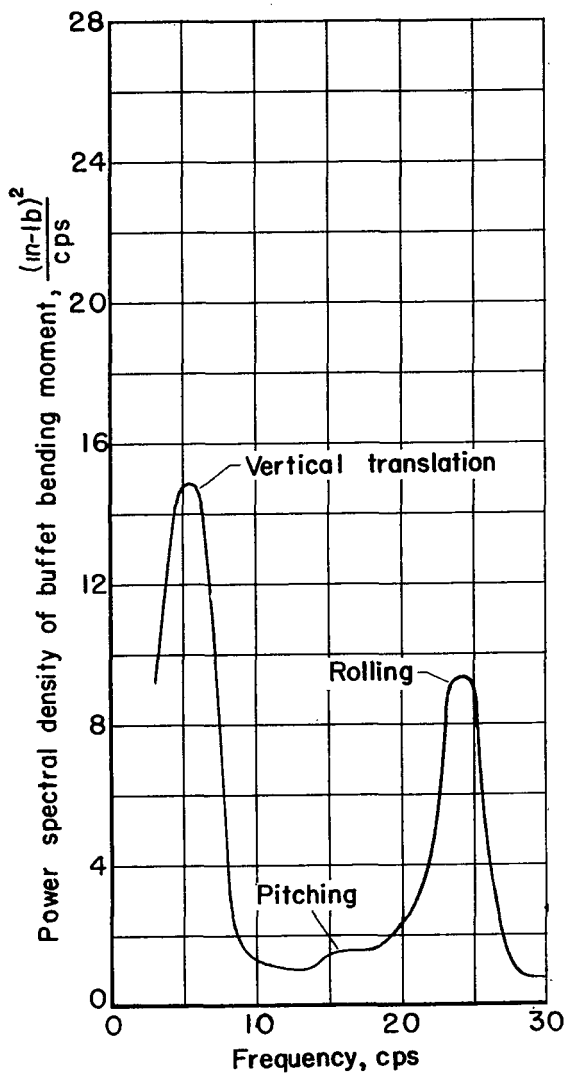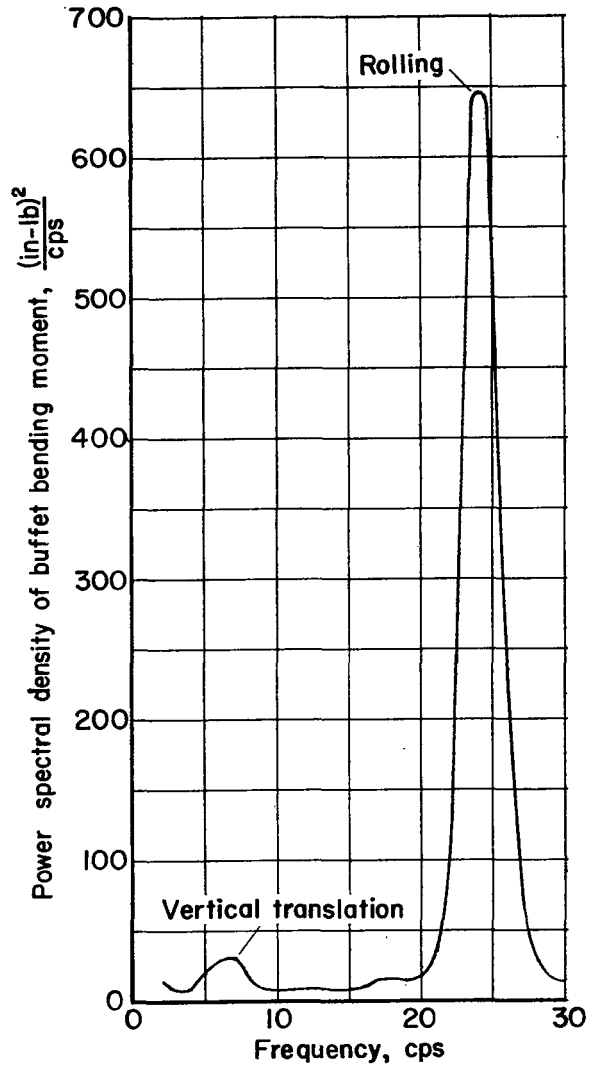
(a) α = 0°.   (b) α = 4°.

Figure 12.- Low-frequency-range spectra of the output of the bending-
    moment gage with a filter band width of 3 cycles per second. Basic
    model at 0.80 atmosphere for M = 0.95 and two angles of attack.
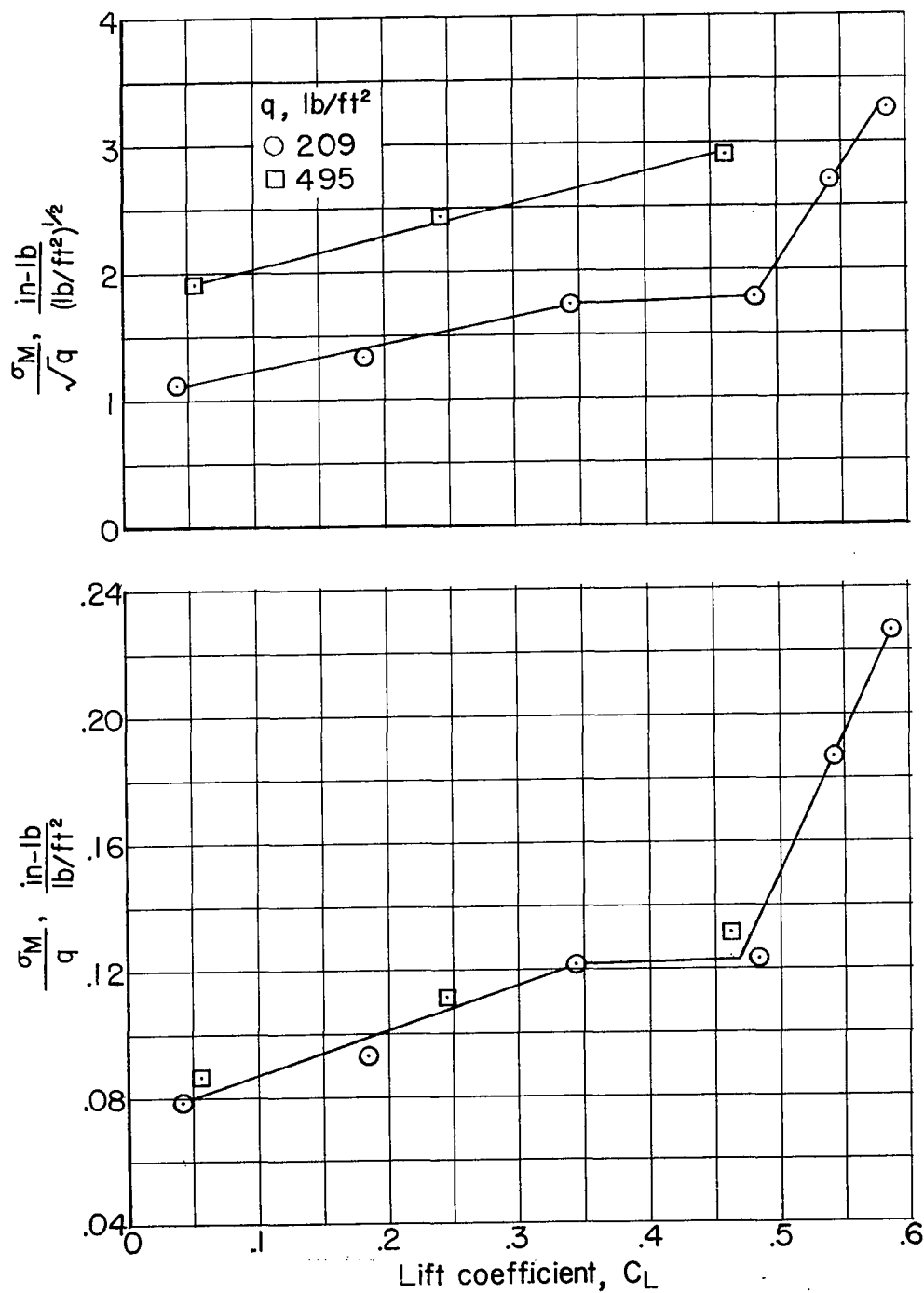
Figure 13.- Effect of density on the buffet bending moment. Basic
model at M = 0.80.
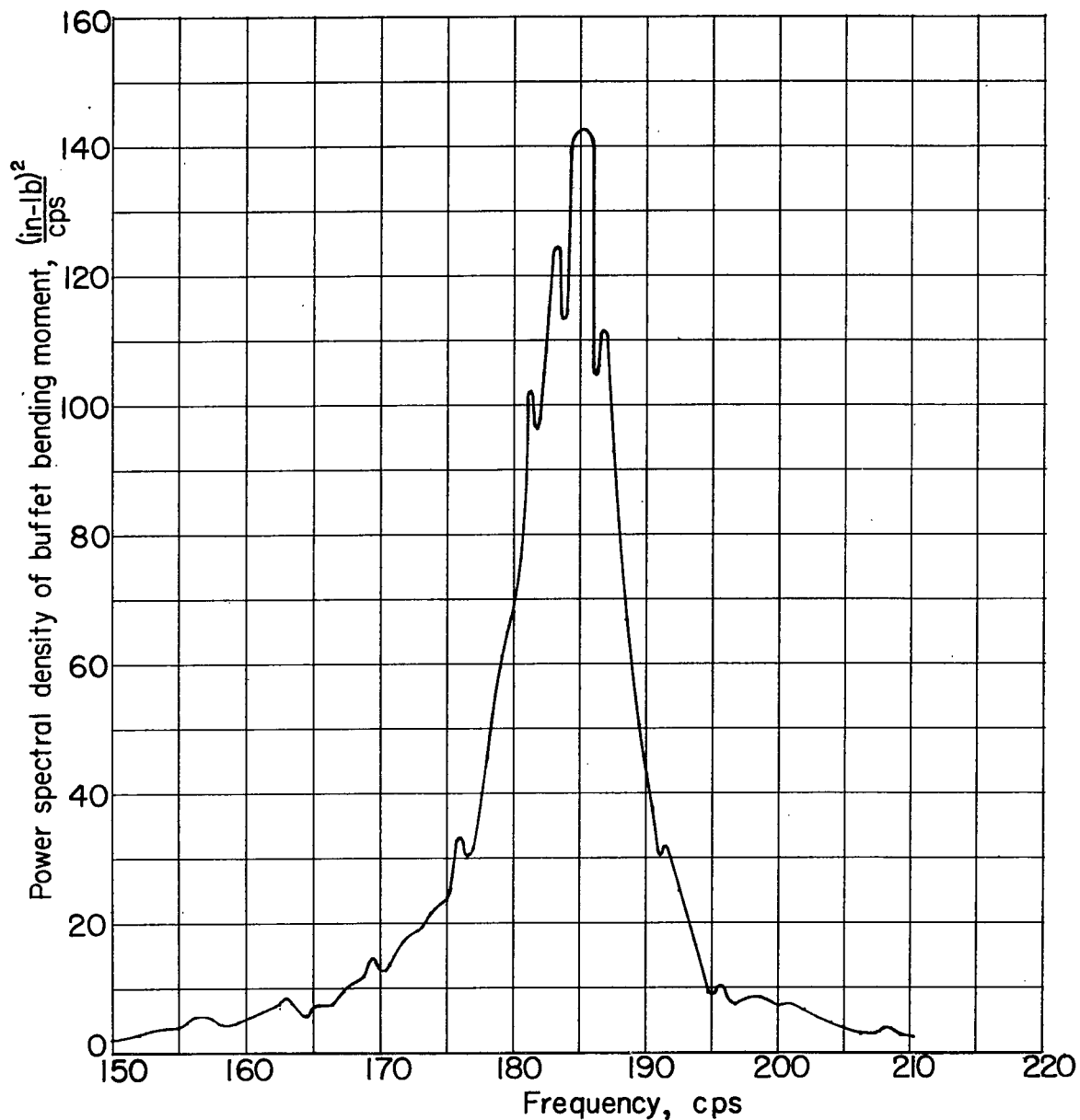
Figure 14.- Typical spectrum in vicinity of wing first bending
frequency with a filter band width of approximately $1\frac{1}{4}$ cycles
per second. Basic model at 0.33 atmosphere for M = 0.95
and $\alpha = 6°$.
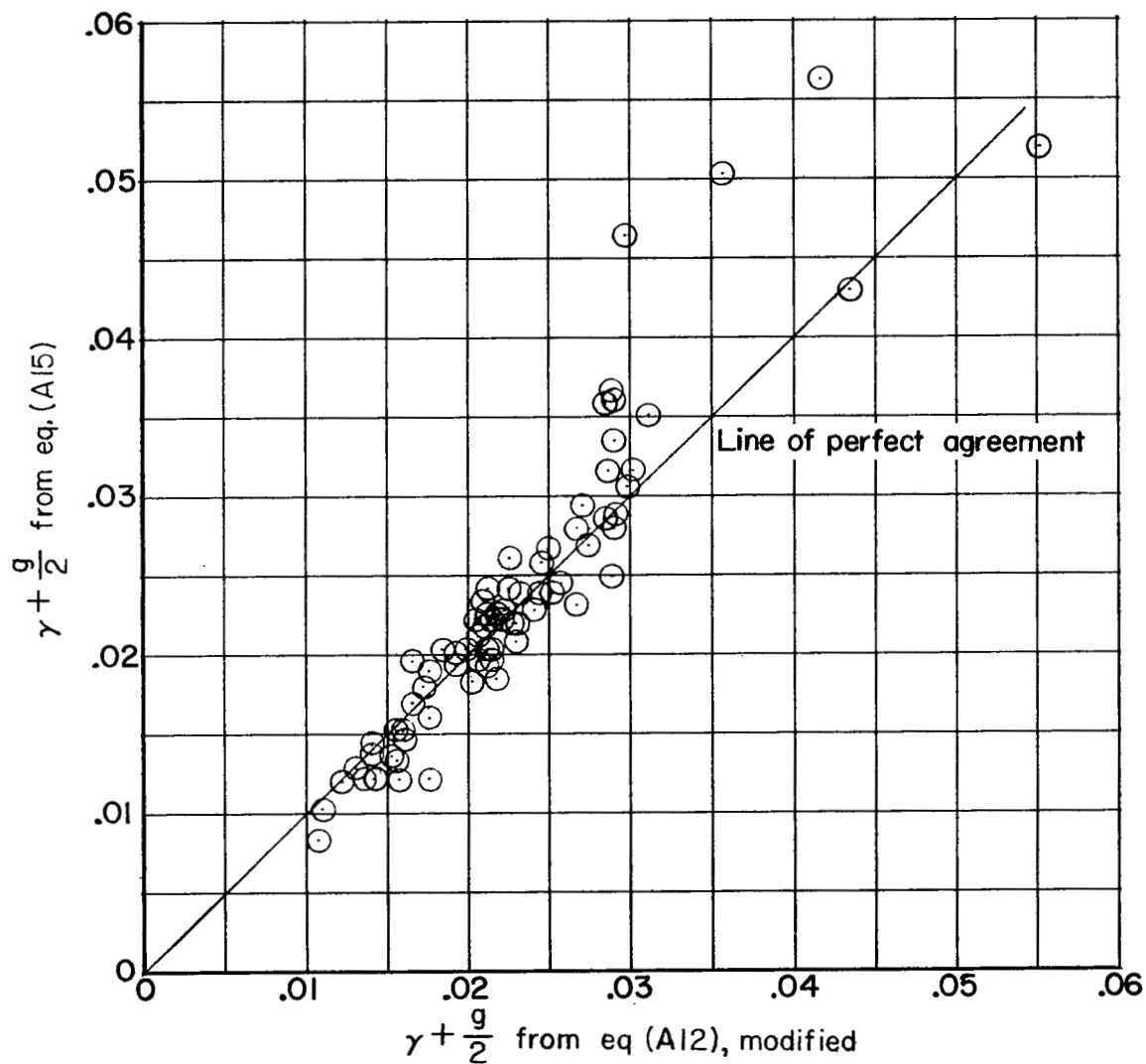
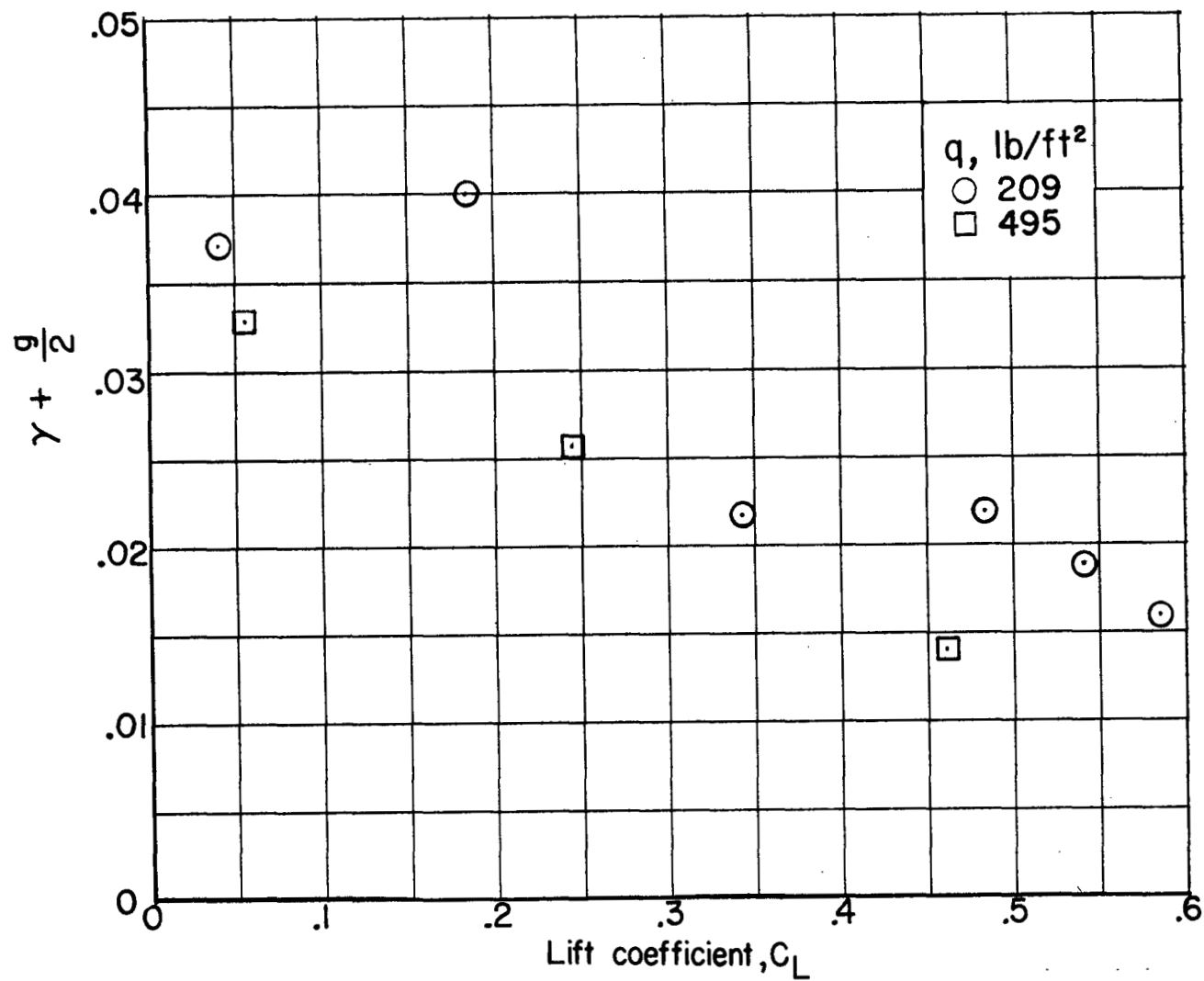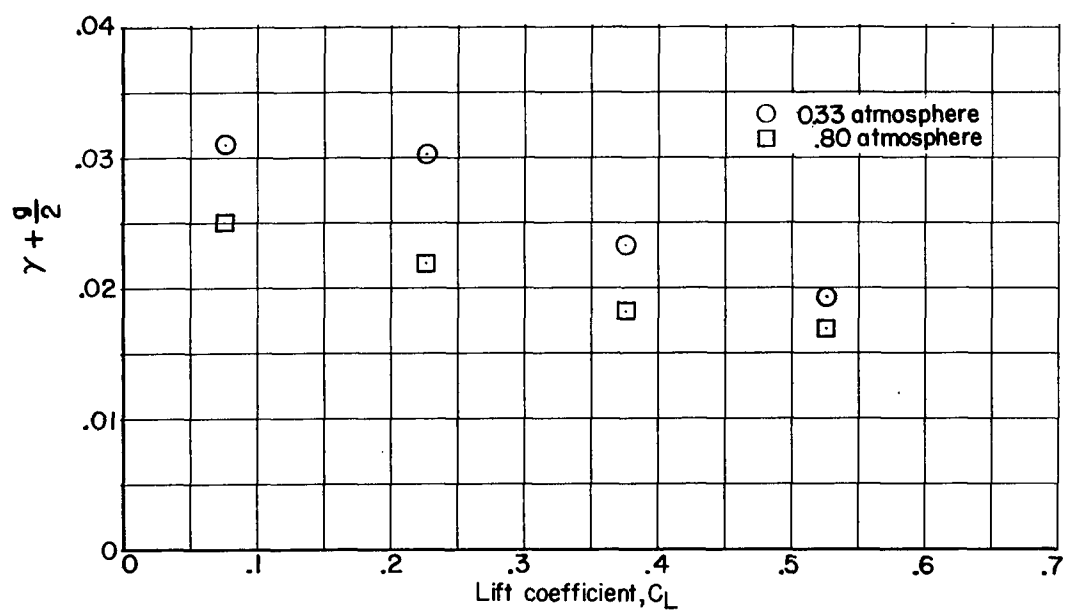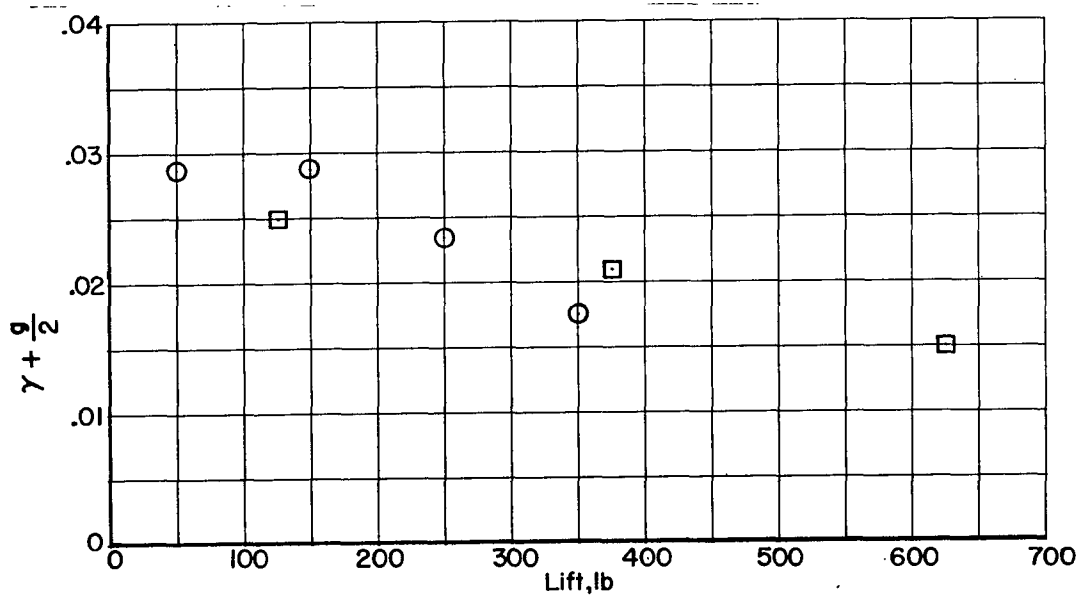Figure 15.- Comparison of total damping coefficients obtained by two
independent methods.

Figure 16.- Effect of density on total damping coefficient. Basic model at M = 0.80.

(a) Lift coefficient.

(b) Lift.

Figure 17.- Variation of total damping coefficient with lift and lift
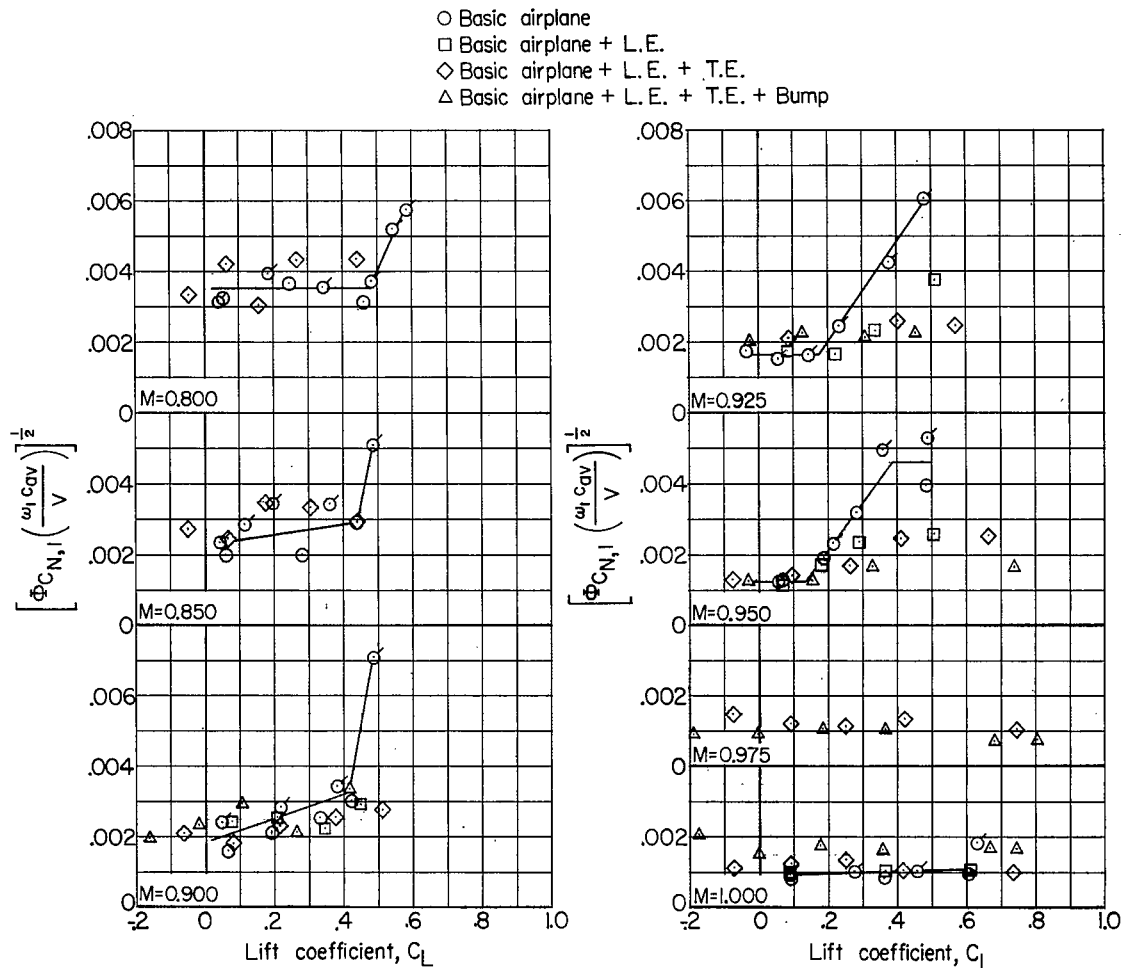coefficient. Basic model.

Figure 18.- Variation with lift coefficient of the square root of the spectral density of the generalized normal-force coefficient at first-mode natural frequency ω_1 for all four configurations. Plain symbols are for 0.80 atmosphere and flagged symbols are for 0.33 atmosphere.